Lithos 302–303 (2018) 242–262

Contents lists available at ScienceDirect

Lithos

journal homepage: www.elsevier.com/locate/lithos

Review article

The Dovyren Intrusive Complex (Southern Siberia, Russia): Insights into dynamics of an open magma chamber with implications for parental magma origin, composition, and Cu-Ni-PGE fertility

Alexey Ariskin [a,b,*], Leonid Danyushevsky [c], Georgy Nikolaev [b], Evgeny Kislov [d], Marco Fiorentini [e], Andrew McNeill [f], Yuri Kostitsyn [b], Karsten Goemann [g], Sandrin T. Feig [g], Alexey Malyshev [d]

[a] Faculty of Geology, Moscow State University, Leninskie Gory 1, 119234 Moscow, Russia
[b] Vernadsky Institute, Kosygin Str. 19, 119991 Moscow, Russia
[c] CODES CoE and Earth Sciences, University of Tasmania, Private Bag 79, Hobart, TAS 7001, Australia
[d] Geological Institute, Sakhyanovoy Str., 6a, 670047 Ulan-Ude, Russia
[e] Centre for Exploration Targeting, School of Earth and Environment, ARC Centre of Excellence for Core to Crust Fluid Systems, The University of Western Australia, 35 Stirling Highway, 6009, Crawley, Perth, Western Australia, Australia
[f] Mineral Resources Tasmania, PO Box 56, Rosny Park, Hobart, TAS 7018, Australia
[g] Central Science Laboratory, University of Tasmania, Private Bag 74, Hobart, TAS 7001, Australia

ARTICLE INFO

Article history:
Received 21 April 2017
Accepted 7 January 2018
Available online 13 January 2018

Keywords:
Yoko-Dovyren
Layered intrusion
Cu-Ni-PGE mineralisation
COMAGMAT-5
Parental magma
Sulphide immiscibility
Open magma chamber
Anomalous mantle source

ABSTRACT

The Dovyren Intrusive Complex (DIC, Northern Baikal region, 728 Ma) includes the layered dunite-troctolite-gabbronorite Yoko-Dovyren massif (YDM), associated mafic-ultramafic sills, and dykes of olivine-rich to olivine-free gabbronorite. Major rock types of the DIC are presented, including a diversity of olivine orthocumulates to olivine-plagioclase and gabbroic adcumulates, carbonate-contaminated ultramafics and Cu-Ni-PGE mineralisation. Detailed comparisons of complete cross-sections of the YDM in its centre and at the NE and SW margins demonstrate differences in the cumulate succession, mineral chemistry, and geochemical structure that likely reflect variations in parental magma compositions. Combining petrochemical reconstructions for most primitive rocks and calculations using the COMAGMAT-5 model, it is shown that the central and peripheral parts of the intrusion formed by olivine-laden parental magmas ranged in their temperatures by 100 °C, approximately from 1290 °C (~11 wt% MgO, olivine Fo88) to 1190 °C (~8 wt% MgO, olivine Fo86). Thermodynamic modelling suggests that the most primitive high-Mg magma was S-undersaturated, whereas its derivatives became S-saturated at T < 1240–1200 °C. These estimates are consistent with geological observations that mostly sulphide-poor mineralisation occurs in the centre of the intrusion, whereas Cu-Ni sulphide ores (locally net-textured) occur in its NE and SW parts, as well as in the underlying peridotite sills. The primitive S-undersaturated olivine cumulates became sulphide-saturated at a post-cumulus stage. As a result, Ni-rich immiscible sulphides formed within and migrated through the early olivine-rich cumulate piles to generate poorly-mineralised plagiodunite. In the troctolite and gabbroic parts of the Dovyren chamber, sulphide immiscibility likely occurred at lower temperatures, producing Cu-rich sulphide precursors, which gave rise to the 'platinum group mineral' (PGM-containing) troctolite and low-mineralised PGE-rich anorthosite in the Main Reef. The geochemical structure of the YDM demonstrates C-shaped distributions of TiO_2, K_2O, P_2O_5, and incompatible trace elements, which are 3–5 fold depleted in the cumulate rocks from the inner horizons of the intrusion with respect to the relatively thin lower and upper contact zones. In addition, a marked misbalance between estimates of the average composition of the YDM and that of the proposed olivine-laden parental magmas is established. This misbalance reflects a significant deficit of the YDM in incompatible elements, which argues that 60–70% of basaltic melts had to have been expelled from the Dovyren magma chamber during its consolidation. A possible scenario of the evolution of the open magma chamber is proposed.

* Corresponding author at: Faculty of Geology, Moscow State University, Leninskie Gory 1, 119234 Moscow, Russia.
E-mail addresses: ariskin@rambler.ru, ariskin@geol.msu.ru (A. Ariskin).

https://doi.org/10.1016/j.lithos.2018.01.001
0024-4937/

Contents

1. Introduction

Sedimentary sequences within the foldbelts surrounding the southern margin of the Siberian Craton host a number of Precambrian large layered intrusions and mafic-ultramafic complexes referred to as the Cu-Ni-PGE East Siberian metallogenic province (ESMP; Polyakov et al., 2013). The ~728 Ma Dovyren Intrusive Complex (hereafter DIC) is located ~60 km NE of Lake Baikal and represents the eastern branch of the ESMP (Fig. 1). The main components of the DIC include the Yoko-Dovyren mafic-ultramafic massif (YDM), underlying ultramafic sills, and associated dykes or sill-like bodies of gabbronorite, both below and above the YDM (Grudinin, 1963, 1965; Gurulev, 1965, 1983; Kislov, 1998; Konnikov, 1986; Yaroshevskii et al., 1982). The main intrusive body (also referred to in the Russian literature as 'the Dovyren intrusion' or simply 'Dovyren') is composed of a succession of ultramafic and mafic rocks ranging from plagioperidotite and dunite to troctolite, olivine gabbro, and gabbronorite. It forms a 26 km long lens-shaped ridge, which is up to ~3.5 km wide in its central part (Fig. 2).

The DIC is one of the best-exposed layered complexes in the world (see below) and, over the last 50 years, it has continued to be a reference site for Russian petrologists dealing with the intra-chamber differentiation of ultramafic magmas and the Cu-Ni-PGE fertility of layered intrusions. This is because of the relatively simple geological setting and uncomplicated internal structure of the YDM (Fig. 2), excellent exposure of complete cross-sections from the bottom to the roof, the occurrence of most known types of Cu-Ni sulphide and PGE-rich mineralisation, as well as Cu-Ni sulphide ores near the bottom

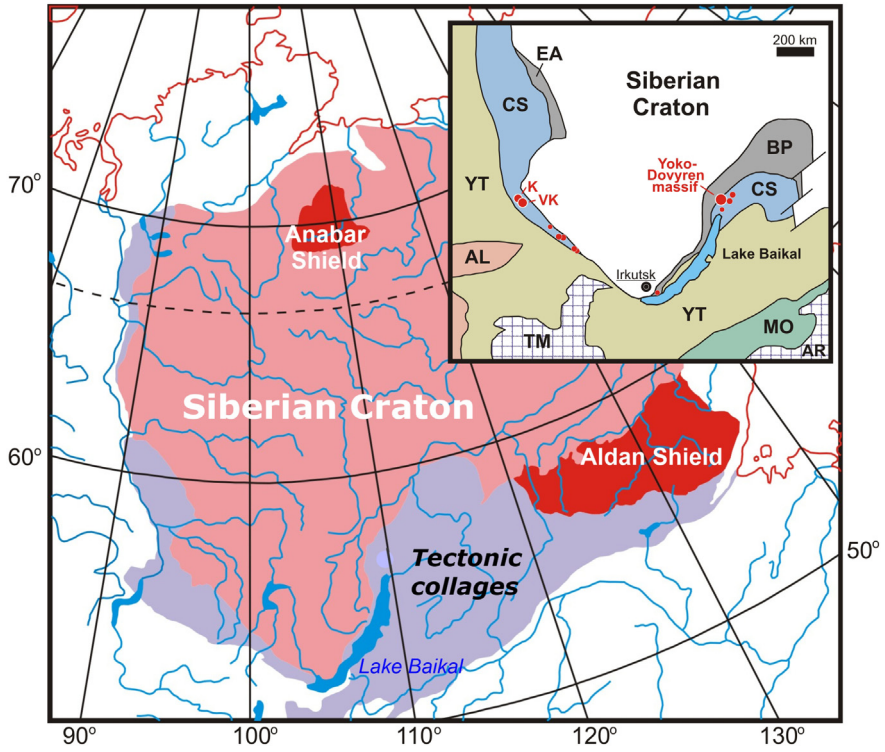

Fig. 1. Major tectonic features of the Siberian Craton and its southern margin. The outline of the Siberian craton includes the Neoproterozoic and older basement (after Parfenov et al., 2010). *BP* 'outer' Baikal-Patom Foldbelt, *EA* East Angara Fold belt. Tectonic Collages: *CS* Circum-Siberia (Proterozoic), *YT* Yenisey-Transbaikal (Vendian through Early Ordovician), *AL* Altay (Vendian through Ordovician), *MO* Mongol-Okhotsk (Devonian through Late Jurassic). Late Proterozoic and Cambrian superterranes: *AR* Argun-Idermeg, *TM* Tuva-Mongolia. The Late Proterozoic intrusions of the southern margin of the Siberian Craton (the East Siberian metallogenic province; Polyakov et al., 2013) are shown by red circles and include: *K* Kingash, *VK* Verkhnii (Upper) Kingash, *YDM* Yoko-Dovyren massif, and other small mafic to ultramafic bodies hosting Cu-Ni-PGE deposits and sulphide ore occurrences.

(e.g., Ariskin et al., 2009, 2016; Balykin et al., 1986; Bolikhovskaya et al., 2007; Kislov, 1998; Konnikov, 1986; Yaroshevskii et al., 1982, 2006).

The DIC is spatially and temporally associated with Inyaptuk-Synnyr volcanics (Manuilova and Zarubin, 1981), which include high-Ti basalts and low-Ti basaltic andesite. The latter are geochemically and isotopically similar to the DIC (Ariskin et al., 2013b, 2015a), suggesting that the low-Ti volcanics are genetically related to the intrusive rocks (Kislov, 1998). The association between the DIC rocks and the low-Ti

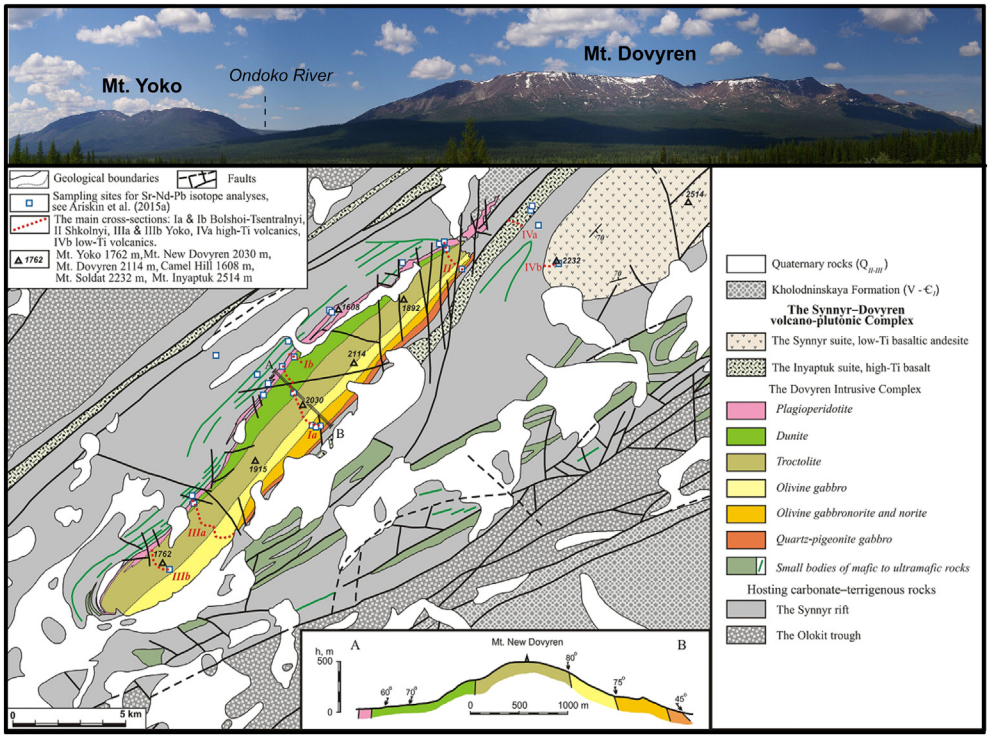

Fig. 2. Photograph of the YDM facing northwest (top) and a schematic geological map of the southwestern termination of the Olokit trough, modified after Ariskin et al. (2013b, 2015a).

volcanics is referred to as the Synnyr-Dovyren Complex (Ariskin et al., 2009), which may be considered as a Late Riphean magmatic province active during the final stages of the Precambrian geological evolution of the southern margin of the Siberian Craton (Kislov, 1998; Konnikov, 1986; Rytsk et al., 2007). This is of particular significance in the context of reconstructions of the geodynamic history of the Siberian Craton during the break-up of Rodinia, which suggest that in the Late Riphean the Siberian Craton was adjacent to northern Laurentia (e.g., Li et al., 2008; Metelkin et al., 2009; Pisarevsky et al., 2008). The Synnyr-Dovyren Complex is contemporaneous to the Franklin event, which formed the large igneous province in Arctic Canada at 723 ± 4.2 Ma (Ernst et al., 2016; Ernst and Bleeker, 2010; Heaman et al., 1992).

The proposed spatial and temporal association of the large igneous provinces (LIPs) in Southern Siberia and Arctic Canada may indicate their similar metallogenic potential, because many intrusive bodies from both provinces contain significant Ni-Cu-PGE mineralisation (Jowitt and Ernst, 2013; Polyakov et al., 2013). The Synnyr-Dovyren Complex and surrounding area was considered as a fertile Ni-Cu-PGE province long before its recognition as the eastern part of the ESMP. Since the late 1950s, Cu-Ni sulphide ores have been discovered within the Yoko-Dovyren (in 1959), Chaya (in 1962), and Gasan-Dyakit (in 1964) massifs (see a review of the Northern Baikal nickel reserves by Kislov, 2010). In 2006–2016, we carried out eight expeditions to the DIC aimed at creating detailed studies of the internal structure of the YDM and its associated sills and volcanics. As a result, a total of 2500 samples have been collected, comprising three complete cross-sections of the YDM (through the central part and at the margins), several cross-sections of the underlying sills, a representative collection of dykes and Cu-Ni-sulphide ores, and several cross-sections through the PGE-rich anorthosites and other mineralised sulphide horizons.

Here we summarise the published information of the DIC (Section 2) and present new data on the structure of the YDM (Section 3) and associated sills and volcanics (Section 4), focussing on the geochemistry of the volcanic-plutonic complex (Section 5) and new data on the low-sulphide and PGE-enriched rocks. The results allow us to reassess the internal structure and various petrological aspects of the YDM, including Cu-Ni-PGE fertility, the compositions of parental magmas, the history of sulphide immiscibility in the cumulate rocks, as well as evidence for an open-system behavior of the Dovyren magma chamber and the nature of an ancient mantle source.

2. Summary of the geology, structure, and fertility of the Synnyr-Dovyren Complex

2.1. Regional geology

The area northeast of Lake Baikal is part of the Baikal Fold Region within the eastern Central Asian Fold belt (Parfenov et al., 2010), which comprises the 'outer' Baikal-Patom Belt at the southern margin of the Siberian Craton and the Baikal-Muya Belt at the eastern margin of the Proterozoic Circum-Siberia folded area (see inset in Fig. 1). Within the Baikal-Patom Belt, the basement rocks are exposed within marginal inliers of the Siberian Craton as blocks of Archean gneisses and Paleo-Proterozoic anorogenic complexes. The Riphean units of the Baikal-Patom Belt comprise several large troughs (e.g., the Patom and Olokit-Bodaibo zones) and uplifted areas (e.g., the Mama Zone; Konnikov, 1986; Rytsk et al., 2007). Geodynamic reconstructions relate the formation of the Olokit-Bodaibo trough to the evolution of the Baikal-Patom paleobasin between the southern margin of the Siberian Craton and the Baikal-Muya paleo-arc during the Proterozoic (Konnikov et al., 1999). More specifically, Middle to Late Riphean mature terrigenous sediments, which include turbidites, carbonaceous shales, carbonates, and volcanics, form the 5–7 km thick Olokit Complex (Rytsk et al., 2002). The structural units within the Olokit Complex comprise sharply asymmetric troughs separated by blocks of elevated basement rocks. The basement rocks below the complex are metarhyolites dated at 1863 ± 5 Ma (Neimark et al., 1990).

Late Riphean collisional processes along the southern margin of the Siberian Craton were accompanied by large-scale sub-horizontal relocations of individual units towards the northeast direction (in the current orientation) and resulted in the formation of the ~150 km long and up to 12–15 km wide Synnyr rift. The Late Riphean rocks of the Synnyr rift (~2.5 km thick) form the top of the Olokit Complex; the uppermost black shale-dominated part of the complex hosts the DIC.

The 3.5 km thick YDM is the main part of the DIC; it forms a ridge comprised of Mt. Yoko (SW) and the much larger Mt. Dovyren (Fig. 2). The YDM is a lens-shaped body with a minimum thickness of ~700 m at its SW termination and is generally concordant with the host sedimentary units and overlying volcanics. The host sediments dip nearly vertically around the YDM, thus exposing the entire cross section of the intrusive and volcanic-sedimentary units. The overlying volcanics include the rocks of the Inyaptuk and Synnyr suites, which form the uppermost units of the Synnyr Rift (Kislov, 1998; Rytsk et al., 2002). The Inyaptuk suite is composed of picritic and basaltic pillow lavas associated with sub-volcanic bodies of trachydacites and rhyolites, whereas the Synnyr suite includes basalts, basaltic andesite, and andesite. These rocks compose the Synnyr Ridge and Mt. Inyaptuk (Fig. 2).

2.2. Geochronology of the DIC and associated volcanics

Hereinafter, we follow rock type specifications presented in Appendices A and B, where analytical methods and whole-rock and mineral compositions are given.

2.2.1. Age of the Dovyren Intrusive Complex

Amelin et al. (1996) suggested that the YDM formed at 673 ± 22 Ma based on the Sm-Nd isotopic compositions of mono-mineralic fractions separated from a gabbronorite from the upper portion of the YDM. These authors also obtained an age of 707 ± 40 Ma for a gabbronorite from a sill beneath the YDM, and a Rb-Sr age of 713 ± 7 Ma from a biotite; however, the Sm-Nd isochron age was considered more reliable. Recent data on U-Pb baddeleyite dating of a pegmatoidal gabbronorite from the YDM yielded an age of 724.7 ± 2.5 Ma (Ernst et al., 2016). Given the uncertainty related to the timing of YDM emplacement, Ariskin et al. (2013b) performed detailed U-Pb dating of zircon from 11 samples, including the YDM rocks (3 gabbronorites and a recrystallised hornfels near the roof), a sulphide-rich gabbronorite dyke near its lower contact, a 200 m thick sill beneath the YDM (the Camel Sill, 5 samples), and an albite hornfels representing low-temperature contact metamorphic facies within the host rocks. Combined together, these data yielded 728.4 ± 3.4 Ma (MSWD = 1.8, n = 99) as the age of the DIC (Fig. 3). This age is consistent with the results of Ernst et al. (2016) and ~55 Ma older than the Sm-Nd isochron age of Amelin et al. (1996).

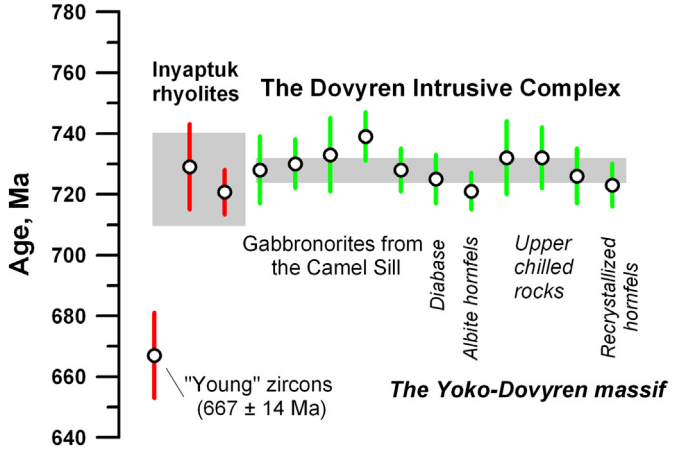

Fig. 3. Geochronology of the Dovyren intrusive rocks and associated volcanics, after Ariskin et al. (2013b).

2.2.2. Age of volcanics and timing of overprinted processes

Ariskin et al. (2013b) performed U-Pb zircon dating on two samples of quartz porphyritic rhyolite from an ~50 m thick dyke cutting through the black shale at the bottom of the Inyaptuk suite, and on a sample of an agglomerate quartz porphyritic tuff overlying the 250 m thick sequence of Inyaptuk basalts. Zircons from the tuff yielded an age of 721 ± 7 Ma (n = 9, MSWD = 1.3), overlapping with the age of the DIC. However, the U-Pb system in some of the zircons from the rhyolite dyke was found to be disturbed. The range observed in the 22 individual analyses was interpreted to reflect the presence of zircon populations corresponding to two discrete events. The age of the first population is 729 ± 14 Ma (MSWD = 0.74, n = 8) overlapping with the age of the DIC, whereas the second population is much younger at 667 ± 14 Ma (MSWD = 1.9, n = 13), likely corresponding to the timing of the hydrothermal alteration that affected the entire Synnyr-Dovyren Complex (Kislov, 1998; see below). The exact age of the low-Ti Synnyr volcanics remains unconstrained; however, given their close structural association and compositional similarity with the YDM, it is believed that they are related to the YDM (Ariskin et al., 2009).

The timing of hydrothermal alteration was assessed by Rb-Sr geochronology carried out on leachates derived from partially- to totally-serpentinised peridotites from the Camel Sill (Appendix A). These samples are characterised by very high Rb/Sr ratios (5.8–7.1), atypical for mafic and ultramafic rocks; the high Rb/Sr values were interpreted to originate during serpentinisation of these rocks. The results suggest that the age of the overprinted process is 659 ± 5 Ma (MSWD = 1.3), which is consistent with the youngest U-Pb age recorded by some of the zircons from the rhyolite dyke, as discussed above.

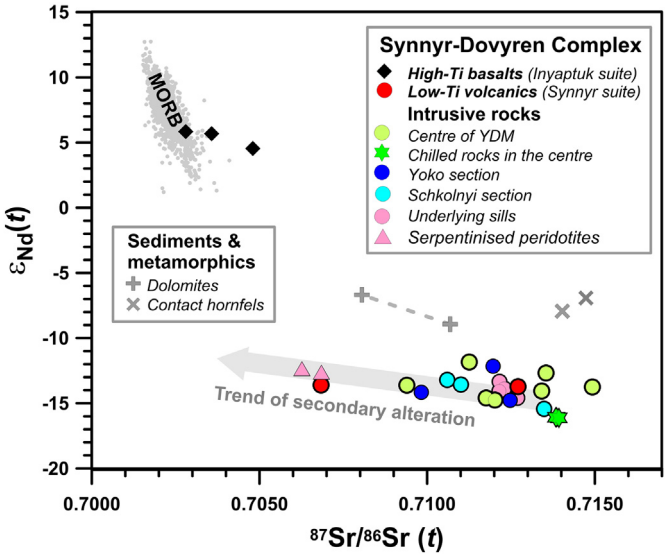

Fig. 4. Sr and Nd isotopic compositions of igneous and sedimentary rocks from the Synnyr-Dovyren complex. All values are corrected to the DIC age of 728 Ma (Ariskin et al., 2013b). The volcanic rocks were sampled along traverses III and IV in Fig. 2. 'Underlying sills' and 'Serpentinised peridotite' include samples from the Camel Sill (Section 4.1). Two sedimentary rocks (referred to as 'dolomites' in the legend) represent dolomitised marbles from the host sedimentary sequence (Amelin et al., 1996). Two samples denoted as 'hornfels' include albite hornfels 07DV163-1 (Ariskin et al., 2015a) and a metamorphosed siltstone shale, TST-28 (Amelin et al., 1996). The 'MORB' field is from Kostitsyn (2004, 2007).

2.3. Sr-Nd isotopic compositions

Radiogenic isotopic compositions of Sr, Nd, and Pb have been analysed in 31 samples from the DIC and associated volcanics (Ariskin et al., 2015a). The examined samples include 14 mafic and ultramafic rocks from the YDM, eight samples from the underlying peridotitic sills, two samples of gabbronorite sampled in the vicinity of the lower YDM contact, a contact albite hornfels, three high-Ti basalts, two low-Ti basaltic andesites, and a low-grade metamorphosed tuffaceous silt from the exocontact of a rhyolite dyke.

The isotopic composition of the high-Ti basalts is similar to the mid-ocean ridge basalt (MORB) source at the time of emplacement, t = 728 Ma (Ariskin et al., 2013b). Unaltered plagiodunite, gabbronorite, and contact gabbronorite from all three studied sections of the YDM display a wide range of $^{87}Sr/^{86}Sr(t)$ ratios (~0.7095–0.7135) and extremely anomalous values of $\varepsilon_{Nd}(t)$ (−11.5 to −15.5; Fig. 4). This range is consistent with the isotopic composition of olivine gabbronorites from the ultramafic sills and a low-Ti sub-volcanic body underlying the Synnyr suite. Another low-Ti basaltic andesite has similar $\varepsilon_{Nd}(t)$ but significantly less enriched $^{87}Sr/^{86}Sr(t)$ (~0.7070). This lower value is likely due to extensive alteration of this rock (Section 2.2.2).

The most important result of these studies is that the maximum 'enrichment' ($^{87}Sr/^{86}Sr(t) = 0.71387 \pm 0.00010$ (2σ), $\varepsilon_{Nd}(t) = -16.09 \pm 0.06$) is found in the lowest marginal rocks of the YDM intrusion, including the chilled picrodolerite (Fig. 4). As far as these rocks represent crystallisation products of the most primitive high-Mg magmas of the YDM (Section 6.1), their anomalous isotopic compositions can be used to propose an ancient mantle source of the parental DIC magmas, as it was argued in Ariskin et al. (2015a) and inferred from the results of this study.

2.4. Main types of YDM cumulate rocks

The YDM was first described in the 1950s during a geological survey of the Northern Baikal region (see Kislov, 2010). This was followed by sampling of representative sections through the intrusion (Balykin et al., 1986; Efimov and Potapova, 2003; Grudinin, 1963, 1965; Gurulev, 1965, 1983; Kislov, 1998; Konnikov, 1986; Konnikov et al., 2000; Yaroshevskii et al., 1982), accompanied by fine-scale mapping of selected areas within the central YDM (Kislov, 1998; Konnikov et al., 2000; Yaroshevskii et al., 1982). The best described cross-section, starting from the Bolshoi and Tsentralnyi creeks in the bottom part of the intrusion (see sections Ia and Ib in Fig. 2), is shown in detail in Fig. 5. This generalised cross-section, which also includes our new data (Section 3), is used to highlight the most important features of the main YDM rock types.

The generalised cross-section through the central YDM (hereafter the Bolshoi-Tsentralnyi section) consists of (I) a 3–5 m thick layer of chilled picrodolerite at the lower contact with hornfels, followed by (II) a basal unit of a plagioclase peridotite up to 150–170 m thick (Gurulev, 1965; Konnikov, 1986). The plagioperidotite gradually transitions into (III) plagiodunite (40–60 m), followed by (IV) a thick layer of low porosity adcumulate dunite (up to 970 m). The dunite zone transitions into (V) a layered sequence of adcumulate melano- to leucotroctolite (~950 m), which contains several layers of clinopyroxene-bearing (up to 5–7% Cpx) troctolite or 'olivine gabbro' (Kislov, 1998) in the upper portion (forming the crest of the Dovyren ridge). Starting from this horizon, the upper part of the YDM contains both veins and schlieren of gabbro-pegmatite, granophyre, and coarse-grained anorthosite (Fig. 6). Along the southeastern slope of the ridge (~2200 m from the lower contact of the intrusion, Fig. 5), modal clinopyroxene increases rapidly leading to a transition from troctolite to (VI) the olivine gabbro zone, ~450 m thick. This is followed by (VII) interbedding of olivine norite and olivine gabbronorite (up to 600 m), which transitions into (VIII) a sequence of pigeonite gabbro and quartz-granophyre gabbronorite (~220 m) near the roof of the intrusion. A thin unit of fine-grained gabbronorite marks the upper YDM contact. The transitions between the main units of the intrusion commonly involve rhythmic intercalation of various rock types. A horizon of poikililic Cpx-containing dunite within the troctolite zone and layers of olivine gabbro among gabbronorite are typical examples of such intercalation.

The detailed structure of the lower contact zone is complicated by the presence of tabular bodies of mafic to ultramafic rocks, which likely represent multiple, nearly coeval intrusive events at the onset of the

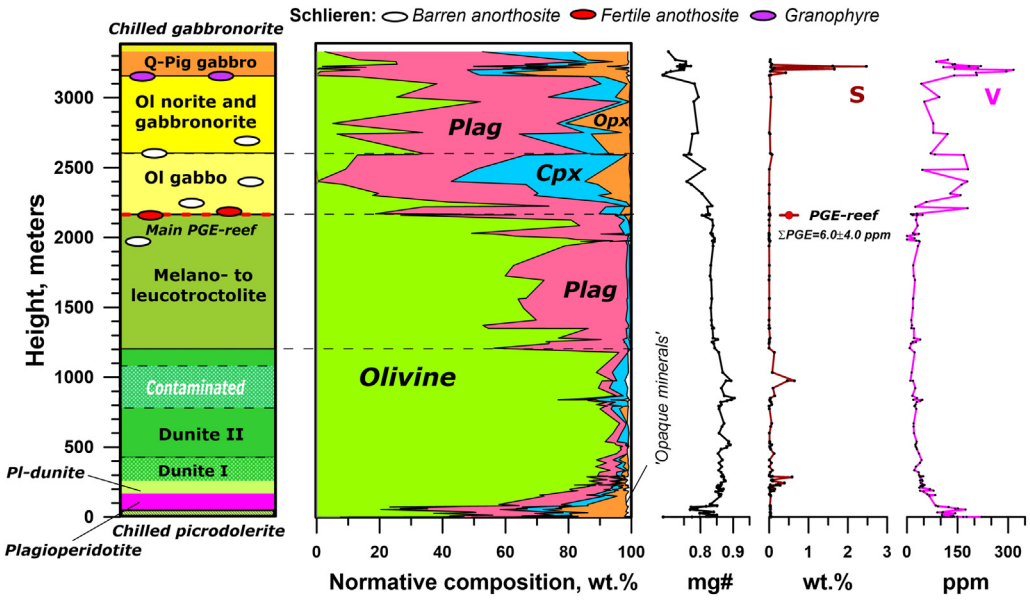

Fig. 5. Structure of the Bolshoi-Tsentralnyi section in the centre of the Yoko-Dovyren massif. Mineral proportions represent normative contents, calculated from whole-rock compositions assuming $Fe^{3+}/\Sigma Fe = 0.05$. S and V concentrations are from our X-ray fluorescence (XRF) analyses (Appendix B, Sheet 'Rocks'), except for the Main PGE-Reef samples, with bulk rock S concentrations taken from Tolstykh et al. (2008).

main emplacement stage. These bodies (often referred to as 'sills') have a thickness of several tens to 200 m and are locally separated by country rocks (Fig. 2). In some places, these sills form an interconnected sequence, allowing for their consideration as apophyses from the basal zone of the intrusion, making it difficult to locate the exact position of the lower YDM contact. A further complication is the occurrence of several large-scale faults cutting the intrusion across and along its strike (Kislov, 1998).

2.5. Magnesian skarns in ultramafics

A distinguishing feature of the YDM is the occurrence of numerous xenoliths of magnesian skarns in dunite and troctolite that are interpreted to be the products of in-situ assimilation of marbles and dolomites by high-Mg magmas during emplacement (Gurulev, 1983; Pertsev and Shabynin, 1979). According to Wenzel et al. (2002), rapid heating of the xenoliths by mafic magma resulted in decomposition of carbonates, releasing CO_2 and CaO into the magma, thus expanding the stability field for Ca-rich clinopyroxene in the surrounding rocks. The magnesian skarns occur as disturbed leucocratic xenoliths, several cm to several m in size, or as undisturbed layers up to 100–150 m long (Fig. 6). In the central YDM these xenoliths are most abundant at a distance of 200–400 m below the contact between dunite and troctolite. Mineralogy of the metamorphic rocks is dominated by brucite pseudomorphs after periclase, forsterite, and aluminous spinel; the

Fig. 6. Xenoliths of Mg-rich skarns within dunite (A); schlieren of anorthosite (B); and a gabbro-pegmatite (C) within the gabbroic part of the YDM.

fine-grained Fo-Sp assemblages can also be associated with the brucite skarns, or observed as isolated schlieren (Pertsev and Shabynin, 1979; Wenzel et al., 2002). It was suggested that these xenoliths mark the pre-intrusion position of the sedimentary carbonates, with their initial location remaining almost undisturbed (Konnikov, 1986).

2.6. Cu-Ni-PGE mineralisation within the DIC

The Cu-Ni sulphide mineralisation within the YDM and associated intrusive rocks ranges from widespread disseminated sulphides to net-textured and massive pyrrhotite-rich ores at the lower YDM contact and within the underlying ultramafic sills and gabbronorite dykes (Ariskin et al., 2016; Kislov, 1998). YDM mineralisation was first described in 1949; however, it was only in 1959–1963 that this area was first subjected to detailed geological prospecting (Tolstykh et al., 2008). Limited-scale surveys were conducted in 1976–1979 and 1986–1993, leading to the establishment of a subeconomic so-called Baikal Deposit, which contains a total of 147, 000 tons Ni, 51,000 tons Cu, and 9500 tons Co (Kislov, 2010). The deposit contains both syngenetic and epigenetic Cu-Ni sulphide mineralisation.

2.6.1. Syngenetic Cu-Ni mineralisation

The syngenetic mineralisation varies from finely-disseminated interstitial sulphides (0.5–3 mm in size, commonly <1% sulphide in the rock) to 'impregnated' (Ariskin et al., 2016) or 'globular' and 'net-textured' ores (Fig. 7A), following terminology by Barnes et al. (2017). All these types are irregularly distributed throughout the entire YDM and associated sills (Kislov, 1998). The most sulphide-rich occurrences (up to 30% sulphides) are typical for ultramafic bodies below the lower contact. These ores generally occur where dykes of gabbronorite cut plagioperidotite and olivine gabbronorite within the sills. Outcrops of this type of sulphide ore were traced continuously for ~1700 m parallel to the lower contact in the YDM centre; the width of the ore lenses varies from 8 to 25 m, locally reaching 80 m (Kislov, 1998). Where it occurs in the gabbronorite, the Cu-Ni mineralisation is observed as disseminated pyrrhotite-rich sulphides that may produce branchy blebs up to 20 mm in size.

Another type of syngenetic mineralisation includes poorly-mineralised rocks with fine Ni-rich (60–95% pentlandite) interstitial sulphides, which occur in a ~150 m horizon within the transition zone from plagiodunite to adcumulate dunite (Fig. 5 and Ariskin et al. (2016)). Near the YDM roof, pyrrhotite-rich sulphide mineralisation is observed in olivine-free gabbronorite and quartz-pigeonite gabbro, with S concentration reaching as much as 3 wt% S (Fig. 5).

2.6.2. Epigenetic Cu-Ni mineralisation

Epigenetic mineralisation is observed in metasomatized and essentially recrystallised rocks, generally as massive and vein-like brecciated ores (Fig. 7B), locally occurring within widespread domains of net-textured sulphides (Kislov, 1998). The largest sulphide lode was discovered in 1959 at the NE YDM contact (the Ozernyi prospect; Denisova, 1961). It extends along the base of the YDM for a distance of 650 m, and is 0.7–1.0 m wide. Smaller lodes (15–50 m long and 0.2–1.5 m thick) are confined to tectonic transgressions demarcated by sills of plagioperidotite and associated dykes. Drilling has demonstrated that the sulphide-rich veins dip nearly vertically and extend to depths of >500 m (Kislov, 2010). The massive ores consist of 70–95% pyrrhotite and contain minor amounts of troilite, pentlandite (7–25%), and chalcopyrite (0.1–6%). These ores contain up to 2.1 wt% Ni, 0.64 wt% Cu, and 0.14 wt% Co (Kislov, 1998).

2.6.3. PGE-rich sulphide-poor mineralisation in anorthosite

Low-sulphide PGE-rich mineralisation within the YDM was first documented within anorthosite near the transition from troctolite to olivine gabbro (Distler and Stepin, 1993; Konnikov et al., 1994; Kislov et al., 1995; Orsoev et al., 1995; Fig. 5). Later, a discontinuous zone of PGE-rich sulphide-poor mineralisation was traced near the basement of the gabbroic subsection along the YDM strike for over 20 km (Kislov, 1998). The highest PGE contents (up to 12 ppm) are found in the central part of the intrusion (the Main Reef) within a 150–200 m zone composed of concordant veins and lenses of coarse-grained and

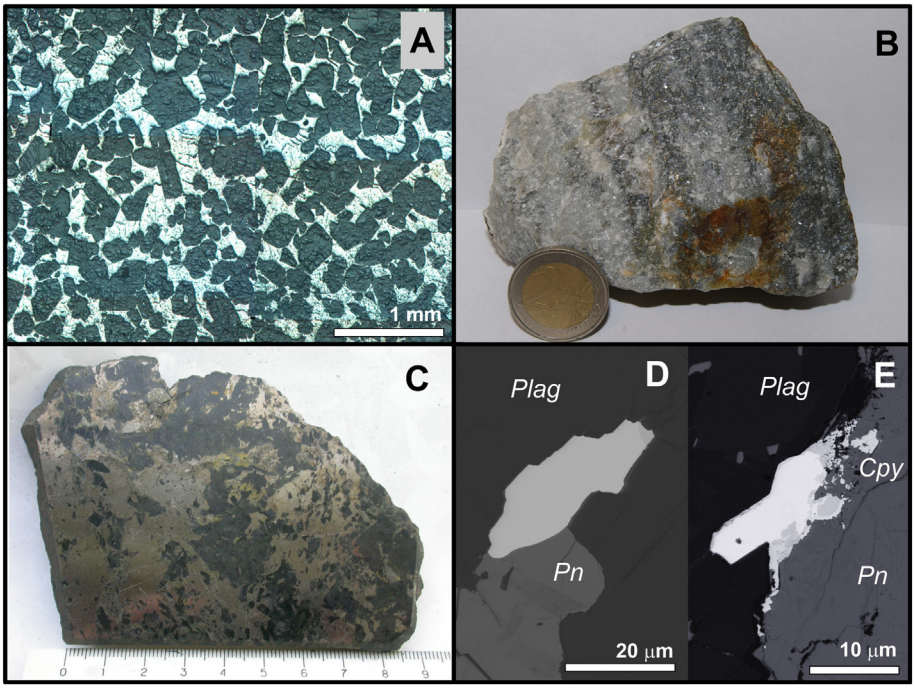

Fig. 7. Sulphide mineralisation of the Dovyren Intrusive Complex. A Net-textured Cu-Ni sulphide ore from a sill below the YDM (sample 07DV107-1); B Low-mineralised PGE-rich anorthosite from the Main PGE Reef (07DV146-1); C A massive Po-rich sulphide ore from the Ozernyi prospect at the NE termination of the YDM (sample provided by D.A. Orsoev, Geological Institute in Ulan-Ude, Buryatia, Russia); D and E Back-scattered electron (BSE) images of Pt-Pd-Ag minerals associated with sulphides: D Moncheite in a thin anorthositic vein (the Main PGE Reef, sample 07DV146-2); E A composite grain of moncheite (light) and telargpalite (grey) in a low-mineralised troctolite (Section 2.6.4).

taxitic troctolite, olivine gabbro, as well as minor leucogabbro and gabbronorite. This highly heterogeneous zone hosts numerous bodies of barren (Fig. 6B) and mineralised anorthosite (Fig. 7B), which occur as large schlieren and lens-like bodies commonly surrounded by sulphide-free or poorly-mineralised gabbro-pegmatite (Fig. 6C). Anorthosite bodies are usually a few cm to 1 m thick and extend for 2 to 5 m along the massif strike (rarely >40 m long), forming a discontinuous sulphide-poor mineralised zone.

The sulphide assemblages are Cu-rich, including chalcopyrite, cubanite, bornite, and in rare cases talnakhite, heazlewoodite, and godlevskite (Konnikov et al., 2000). Pentlandite and pyrrhotite are minor phases (<15–20 vol% in total). Using a combination of hydroseparation of finely-crushed sulphide-poor anorthosite (Orsoev et al., 2003; Rudashevsky et al., 2003) and scanning electron microscopy (SEM) studies of the mineralised samples (Tolstykh et al., 2008), approximately 80 grains of precious metal minerals were found. The PGMs range in size from 1 to 2 to 60 μm, with moncheite (Fig. 7D), potarite, and tetraferroplatinum being predominant. Minor PGMs included kotulskite Pd(Te,Bi,Pb), sobolevskite Pd(Bi,Te), and a number of Ag-minerals (argentite Ag_2S, stephanite Ag_5SbS_4, amalgam AgHg). Additional studies of three anorthosite samples from the Main Reef revealed the presence of 22 PGM grains (~2–35 μm), including moncheite $(Pt,Pd)(Te,Bi)_2$, paolovite $(Pd,Pt)_2(Sn,Te)$, atokite (Pd,Au)(Sn,As,Sb), and merenskyite $Pd(Te,Bi)_2$-$Pt(Te,Bi)_2$ (Ariskin et al., 2016).

Despite the sulphide-poor character of the Main Reef mineralisation, the amount of PGE-bearing sulphides in the anorthosite may locally reach up to 3–5 vol%. Due to such irregular distribution of sulphides, the total concentration of PGE + Au in the rock varies in the range 0.3–12.1 ppm at 0.006–0.710 wt% Cu and 0.023–0.430 wt% Ni (Tolstykh et al., 2008). Laser ablation inductively coupled plasma mass spectrometry (ICP-MS) analysis of sulphide phases from the PGE-mineralised anorthosite revealed very high concentrations of Pd in pentlandite (235 ± 84 ppm) which also contains 6.9 ± 6.5 ppm Rh, 1.9 ± 2.0 ppm Ir, 0.93 ± 0.64 ppm Ru, 0.55 ± 0.30 ppm Os, 0.30 ± 0.12 ppm Re, 34.8 ± 12.1 ppm Ag, and 25.1 ± 15.5 ppm Te (Ariskin et al., 2016).

2.6.4. Recently discovered PGM-containing troctolite

Geochemical and mineralogical evidence for the presence of PGM-bearing low-sulphide occurrences within troctolite was first presented by Ariskin et al. (2015b). A troctolite collected ~120 m above the dunite/troctolite boundary along the stream of Tsentralnyi Creek contained Cu-rich sulphides with minor pentlandite, which is highly enriched in Pd (91 ± 84 ppm, n = 7; max 250 ppm). This is similar to the average 235 ppm Pd value observed in pentlandite from the Main PGE Reef. High-resolution SEM analysis revealed the presence of 12 grains of PGMs (mainly Pd bismuth-tellurides, 1–9 μm in size) and two grains of electrum (up to 8 μm in size). A more detailed sampling of the lower troctolite horizon revealed a zone of weakly-altered mesocratic troctolite ~250 m above the dunite/troctolite boundary, which contained disseminated round silicate-sulphide clusters, several cm to ~10 cm in diameter.

In thin sections, these heterogeneous schlieren displayed typical orthomagmatic intercumulus sulphides filling the pore space between olivine and plagioclase crystals (Ariskin et al., 2015b). Similar to the Main PGE Reef, chalcopyrite and cubanite accounted for ~75–80% of the total sulphide in the samples. As many as 60 PGM grains (1 to 40 μm in size) were identified in two samples from this new occurrence. Further analyses of the 30 largest grains by high-resolution SEM revealed the presence of PGM assemblages (Fig. 7E), which are generally similar to those observed in the Main Reef anorthosite. Tellurides and bismuthotellurides of Pd, Ag, Pt, and Pb are the most abundant phases (moncheite, paolovite, atokite, merenskyite, michenerite $Pd_2(Bi,Te)$, kotulskite Pd(Te,Pb,Bi), and telargpalite $(Pd,Ag)_3Te$). In addition, native alloys/amalgams, such as electrum (Au-Ag), tetraferroplatinum (PtFe), and potarite (PdHg) are present. Minor PGMs include zvyagintsevite Pd_3Pb and taimyrite $(Pd,Cu)_3Sn$. Chemical analyses of pentlandite from these samples demonstrated high concentrations of all PGE with the notable exception of Pt (all values in ppm): Pd 23.1 ± 7.2, Rh 23.1 ±7.2, Ru 7.5 ± 4.7, Os 4.2 ± 3.3, and Ir 6.7 ± 4.0 (Ariskin et al., 2015b).

3. Detailed structure of the Yoko-Dovyren massif

We summarise below the petrographic descriptions of Kislov (1998) and Ariskin et al. (2009, 2016) and present new data on chemical compositions of minerals and rocks from three cross-sections through the YDM, which are important for the following discussion on the origin and parental magma compositions of the DIC.

3.1. The Bolshoi-Tsentralnyi cross-section

3.1.1. Chilled rocks at the lower contact

Directly at the lower YDM contact, a ~3–5 m thick zone is composed of magnesian gabbronorite and picritic rocks (compositionally olivine gabbronorite) with variable amounts of cumulus olivine and subophitic textures of their groundmass. The chilled gabbronorite is composed of fine-grained fibrous aggregates of altered plagioclase and clinopyroxene, bronze to brown mica (mostly phlogopite with MgO/FeO > 2), and rare resorbed olivine crystals. Plagioclase and clinopyroxene commonly form zoned laths, whereas phlogopite mostly forms oikocrysts. Rare idiomorphic grains of chromite and apatite are also present.

Transition from the chilled gabbronorite to the more ultramafic lithologies inward of the intrusive body is marked by the appearance of subhedral, more-abundant grains of olivine (0.4–2 mm), resulting in a porphyritic texture. A large amount of thin plagioclase laths leads to the ophitic texture of the groundmass (Fig. A1A in Appendix A). In the Russian literature these rocks were variably described as 'ophitic gabbro' (Gurulev, 1983) or 'picrodolerite' (Kislov, 1998), focussing on the gradual change from aphyric rocks with 10–11 wt% MgO at the very contact, towards olivine-phyric coarse-grained rocks with 17–22 wt% MgO several meters above (Fig. 8, Appendix B, Sheet 'Rocks'). The textural features indicate that picrodolerite formed via fast cooling of a high-Mg magma, suggesting that the rocks are orthocumulates crystallised from olivine-laden YDM parents (Ariskin et al., 2003, 2009). Typical mineralogy of the picrodolerite is shown in Fig. 9, with details given in Appendix A and average compositions listed in Appendix B.

3.1.2. Basal plagioperidotite

Olivine-rich ortho- and mesocumulates, often referred to as 'plagioclase peridotite' (Kislov, 1998) or 'plagioclase lherzolite' (Tolstykh et al., 2008), contain up to 37 wt% MgO (Appendix B, Sheet 'Rocks') and comprise a ~160-m-thick basal unit. In fact, these rocks represent a diversity of olivine gabbronorite ranging from moderately (25–40 vol% Ol) to highly melanocratic varieties (65–75 vol% Ol). This type of rock first appears within 5–10 m from the contact and displays rapidly cooled ophitic textures, although less magnesian picrodolerite is also present at that level. The transition from picrodolerite to plagioperidotite is recorded by a gradual decrease in phlogopite and increase in olivine, which is accompanied by a transformation of the groundmass texture from ophitic to poikilitic and then hypidiomorphic. Cumulus olivine compositions vary between samples (Fo74-86), whereas intercumulus material contains of compositionally-variable plagioclase (An52-86), magnesian clinopyroxene (mg#86.4 ± 1.3), othopyroxene (mg#84.4 ± 1.0), and phlogopite (mg#80-86), as documented in Appendix B. Cr-spinel occurs as inclusions in olivine and in the intercumulus (see variations in cr# and mg# in Fig. 9).

The chemical compositions of the fresh and moderately-altered (LOI < 5%) plagioperidotite allowed their separation into two major types (Ariskin et al., 2016): the high-mg# Type I and the low-mg# Type II. This is clearly seen on the FeO-MgO diagram (Fig. 8B), where

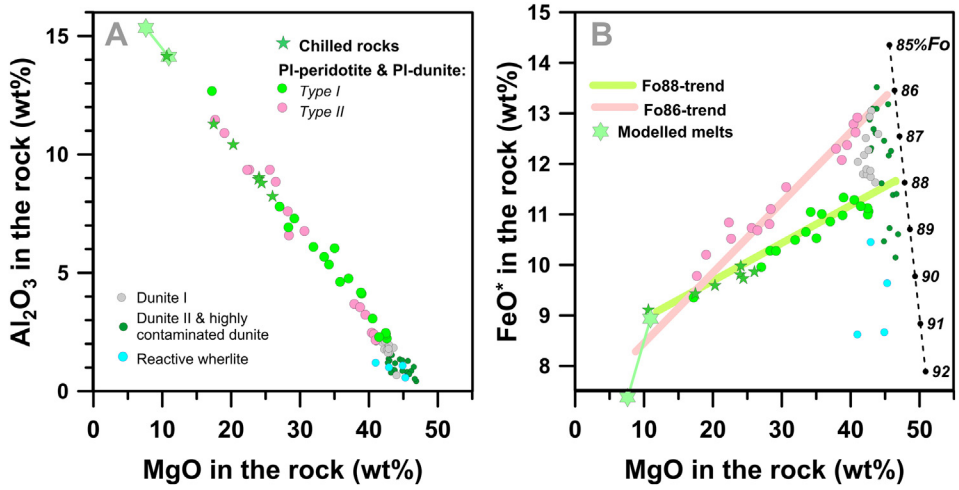

Fig. 8. Whole rock major element compositions of mafic to ultramafic rocks from the YDM basal units in the centre of the intrusion (see Appendix B, Sheet 'Rocks'). Chilled rocks (gabbronorite to picrodolerite), plagioperidotite and plagiodunite, sampled at the distance 0.1–320 m from the lower contact, form two distinct trends in the FeO-MgO diagram, indicating accumulation of olivine ~Fo88 in Type I rocks (Fo88-trend) and ~Fo86 in Type II rocks (Fo86-trend). Except for seven chilled rocks (green stars), other ones are interlayered in a scale of tens meters. Note that the two types cannot be distinguished from their petrography (Fig. A1B and C) or using other major elements (Al_2O_3 in Fig. 8A is shown as an example). Modelled melts represent two compositions calculated at 1285.4 and 1189.7 °C (see Section 6.1).

Type I rocks form a trend towards the composition of olivine ~Fo88 ('Fo88-trend'), whereas Type II compositions extend towards olivine ~Fo86 ('Fo86-trend'). Other major elements presented in terms of MgO display well-defined single trends suggesting that the rocks reflect variable degrees of olivine accumulation in the primitive melts (e.g. Al_2O_3 vs. MgO in Fig. 8A). All samples from the chilled margin plot together with Type I plagioperidotite along the Fo88 trend (Fig. 8B). In addition to plagioperidotite, the basal unit includes rare thin veins (several cm) and thicker layers (up to 1–2 m) of more leucocratic gabbronorite with up to 60–70 vol% plagioclase. Fe-Mg silicates in these rocks commonly have mg# < 82-83, indicating that the rocks represent a more evolved magmatic material formed during in-situ solidification of the host peridotitic unit.

3.1.3. Plagiodunite

The collective term 'plagiodunite' (or Pl-dunite) is applied to olivine-rich rocks (80–85 vol% Ol, 10–12 vol% Pl, <5–6 vol% Cpx + OPx; Fig. A1D), which compose an horizon up to 60 m in thickness that overlies the plagioperidotite horizon. A gradual transition between these two types occurs over an interval of 20–30 m, where the amount of pyroxene oikocrysts decreases up the section. These changes in mineralogy are correlated with depletion in Ti, K, P, and other incompatible elements (Appendix B, Sheet 'Rocks'), suggesting that these changes are due to decreasing porosity of the Ol-rich cumulates (Ariskin et al., 2009). Olivine compositions vary between Fo84-87 (Fig. 9), with plagioclase (An70-77) becoming the main poikilitic mineral (Fig. A1D). Occasional clinopyroxene is present in some interstices, whereas orthopyroxene is observed as thin rims around olivine crystals or as very rare oikocrysts. Cr-spinel is texturally and compositionally similar to plagioperidotite, whereas sulphide is rare (Appendix A). Similar to plagioperidotite, the whole-rock Pl-dunite compositions fall onto the Fo88 and Fo86 trends (Fig. 8B). Based on a combination of the petrographic features and the major element data, we define the transition from the plagiodunite to the overlying Pl-containing dunite (<5–7% Pl) as MgO 39–40 wt%, calculated on the volatile-free basis.

3.1.4. Dunite zone

In the central YDM, a thick zone of dunite is present (up to 970 m, Fig. 5). These rocks contain 90–97 vol% olivine. The boundary between plagiodunite and dunite is gradual, with the amount of intercumulus

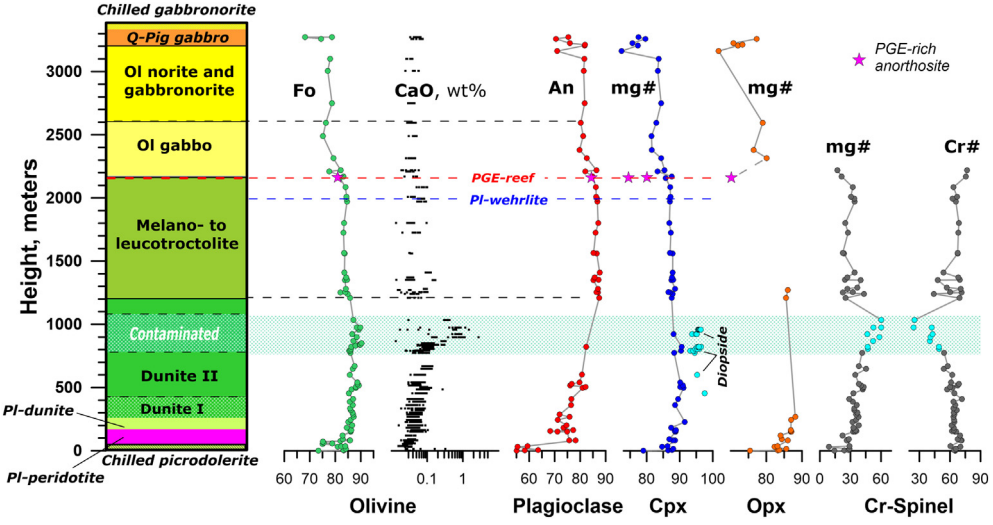

Fig. 9. Variations of mineral compositions along the Bolshoi-Tsentralnyi cross-section. The complete mineral compositions are listed in Appendix B; mg# = MgO/(MgO + FeO), cr# = Cr/(Cr + Al).

decreasing upward. The lowest 20–50 m of the dunite zone are composed of layers of poikilitic rocks relatively enriched in the plagioclase intercumulus (hereinafter dunite I rocks, which are locally similar to plagiodunite) separated by horizons of hypidiomorphic granular dunite (Fig. A2A). As the amount of cumulus olivine continues to increase, panidiomorphic texture develops, displaying linear boundaries of olivine crystals, which meet at ~120° triple points (Fig. A2B; dunite II). This is typical of adcumulates and is accompanied by a further decrease in the proportion of intercumulus phases from 10 to 15 vol% to <5 vol%. At ~450 m above the lower contact, the dunite is effectively a monomineralic olivine adcumulate with chromite inclusions, rare plagioclase interstices, and very thin rims of pyroxene. Their chemical compositions are characterised by MgO > 44 wt% and Al_2O_3 ≤ 1 wt% on an anhydrous basis (Appendix B, Sheet 'Rocks').

This olivine adcumulate comprises a texturally homogeneous zone up to 400 m in thickness (Fig. 5). The entire dunite succession displays minor olivine compositional variations with a subtle tendency towards upward increase in Fo contents (Fig. 9; Appendix A). In several cases, Cpx-filled interstices were found in the lowest porosity olivine cumulates. Such clinopyroxene is generally rich in diopside (Di) (<0.5 wt% Al_2O_3; very high mg#94-97.5 and CaO 25.6–26.6 wt%; Appendix B, Sheet 'CPX'). The amount of Di-rich clinopyroxene increases towards a zone of highly-contaminated dunite and reactive wehrlite, where such high-Ca pyroxene may coexist with a fassaite-like Cpx. Plagioclase composition in the lower dunite I (An 69-81) is commonly less calcic compared to that in the overlying adcumulate dunite II (~An78, see Appendices A and B).

On the Al_2O_3-MgO diagram (Fig. 8A), the dunite I and dunite II compositions extend the general trend defined by plagioperidotite and plagiodunite to lower Al_2O_3 and higher MgO contents. In the FeO-MgO diagram (Fig. 8B) these two types of dunite reveal subparallel trends with respect to the olivine stoichiometry linearisation, with dunite I rocks spanning the whole compositional range between Type I and Type II plagiodunite. This may indicate a genetic link between dunite I and the underlying plagiodunite via a process that combines in situ crystallisation of the original ortho- to mesocumulates followed by their compaction (Ariskin et al., 2009). The higher Fo in dunite II likely reflects the localised assimilation of carbonates, which is recorded in the anomalous mineral compositions (Fig. 9). It is also recorded in relatively low NiO (less 0.15 wt%) at higher Fo (88–90 mol%) in olivine from dunite and wehrlite closely associated with xenoliths of magnesian skarn (see olivine compositions at 974 and 975 m heights in Appendix B).

3.1.5. Highly contaminated dunite

The impact of carbonate assimilation on dunite II compositions was assessed by detailed analyses of rocks along a ~200 m long section starting from ~560 m above plagiodunite. This section includes a gradual transition from 'weakly contaminated' dunite II through to 'highly contaminated' dunite, Di-containing reactive wehrlite and diopsidite, as well as the uncontaminated dunite II adcumulate above this zone of magnesian skarns. Overall, major element rock and mineral compositions are similar in contaminated and uncontaminated dunite II (Appendix B).

Distinctive features of the contaminated dunites are the very high CaO contents in olivine, which may exceed 1 wt% (Fig. 9), and the gradual enrichment in the amount of Di-rich clinopyroxene towards contacts with magnesian skarns. Near the contacts, a fassaite-rich clinopyroxene with 5.5–6.6 wt% Al_2O_3 is common. The amount of Di-rich clinopyroxene in the highly-contaminated rocks may exceed 20–30 vol%, resulting in dunite grading into reactive wehrlite with a poikilitic texture (Fig. A2C), which locally contains small inclusions of calcite. In the sampled area, the strongly serpentinized wehrlite horizon is ~25 m thick. Locally, Di-rich clinopyroxene forms patches and irregular veins of diopsidite within wehrlite and dunite, giving rise to a taxitic texture in the contact rocks.

The highly-contaminated dunite also displays relatively low-cr# and high-mg# spinel compositions compared to spinels in the uncontaminated dunite II (Fig. 9 and Appendix B, Sheet 'SPIN'). The most Cr-depleted spinel occurs 20–50 m above the wehrlite horizon. Schlieren of even more aluminous chromitites (cr# 0.22-0.23) are abundant within the contamination zone (Pushkarev et al., 2004). These schlieren are 10–20 cm wide and up to 0.5–1 m long and contain up to 40–60 vol % of 3–5 mm idiomorphic Al-rich chrome spinel crystals (Fig. A2D). Above the wehrlite, the amount of Di-rich pyroxene in the contaminated rocks decreases together with decreasing Ca and Al in Cpx, until the mineral chemistry becomes similar to that from uncontaminated dunite II below the horizon of carbonate xenoliths. This change is accompanied by a decrease in Fo and CaO contents in olivine (Fig. 9). The uppermost dunite of the dunite zone is generally similar to that classified as 'normal' or 'weakly contaminated' dunite II below the contaminated horizon.

3.1.6. Adcumulate and Cpx-bearing troctolite

The contact between dunite and troctolite is located ~1200 m above the lower YDM contact (Fig. 5), with only one mapped outcrop near the source of Tsentralnyi Creek in the central YDM (profile Ib in Fig. 2). This contact appears as a transitional zone ~100 m thick, marked by the first occurrence of intercalated layers of melanoctratic troctolite and Pl-bearing dunite. The thickness of these layers varies from tens of cm to several meters. Above this level, the amount of troctolite (see textures in Fig. A3), thickness of individual layers, and the amount of plagioclase in troctolite all generally increase, reaching their maximum next to the upper troctolite boundary. However, dunite-like rocks still occur through the upper troctolite zone (Fig. 5). In its upper part, these rocks form several narrow horizons enriched in clinopyroxene ('poikilitic plagiowehrlite' after Konnikov, 1986). The taxitic texture of the plagiowehrlite is distinctly different (Fig. A3D). It is composed of 85–90% olivine and a matrix of Cpx-oikocrysts with rare poikilitic plagioclase.

Most olivine crystals demonstrate a panidiomorphic granular texture; however, smaller, rounded, likely resorbed olivine grains are also present within clinopyroxene. The composition of plagioclase is similar to that of the hosting troctolite. Overall, such dunite-like rocks are similar to troctolite in their mineral chemistry (Fig. 9; see Appendices A and B for details). This is evidence for the plagiowehrlite to have initially been a higher porosity Ol-Pl cumulate depleted in the cumulus plagioclase. Our detailed sampling of the entire troctolite zone suggests that both plagiowehrlite and leucotroctolite to the lowermost anorthosite are principal components of the troctolite unit, which shows extreme phase separation in its upper transitional zone (Figs. 5 and 9).

3.1.7. Zone of olivine gabbro

The gabbroic part of the YDM above the troctolite zone is ~1200 m thick and can be subdivided into three units. The first unit is ~430 m thick and begins directly above the main PGE-rich horizon as an interbedding of rare layers of Cpx-containing troctolite and more abundant olivine gabbro (Fig. 5). It is characterised by an upward decrease in the amount of olivine and general enrichment in clinopyroxene, with the Cpx maximum observed at ~300 m above the irregular contact with troctolite. Another distinctive feature of the olivine gabbro is the occurrence of numerous schlieren of anorthosite and veins of leucogabbro and gabbro-pegmatite with a taxitic texture. On average, the amount of the anorthosite schlieren decreases upwards, whereas veins of gabbro-pegmatite become more abundant.

The textural position of clinopyroxene in the olivine gabbro is variable. In the lowermost Cpx-poor rocks this mineral occurs mostly as an unevenly distributed intercumulus material (Fig. A4B), whereas in the Cpx-rich varieties it is present as relatively large sub-idiomorphic poikilitic grains with rims that occupy the interstices of olivine and plagioclase crystals. Unlike ultramafic YDM rocks, olivine gabbro is characterised by a nonmonotonic upward decrease in the mg# of

mafic minerals and the An content of plagioclase (Fig. 9). A distinctive feature of the olivine gabbro and other gabbroic rocks in the centre of the YDM is the absence of Cr-Al spinel. Only few small spinel grains (mg#13-30, cr#72-79) were found in plagioclase from the lowermost olivine gabbro.

3.1.8. Olivine norite to gabbronorite and near-roof rocks

Above the olivine gabbro, there is an ~530 m thick zone, which contains intercalated horizons of olivine norite and olivine gabbronorite. These units demonstrate a complex layering dominated by olivine gabbronorite. Both types of rocks display gabbroic textures (Fig. A4AC). The mineral assemblage includes ovoid olivine grains (Fo76-79), short tabular plagioclase crystals (An81), and prisms of clino- and orthopyroxene. The occurrence of large oikocrysts and small subhedral grains of orthopyroxene is typical; rare phlogopite is also present. Clinopyroxene has mg#~81 and orthopyroxene mg#~79.

At a distance ~250 m below the upper YDM contact, olivine norite and gabbronorite transition into a sequence of leucocratic quartz gabbro and granophyric gabbronorite (Figs. 5 and 9). These rocks include both intercumulus and sub-idiomorphic grains of inverted pigeonite as their common feature. The low-Ca clinopyroxene is distinguished by a characteristic texture originated via subsolidus decomposition of the original solid solution into lamellae of high-Ca clinopyroxene hosted by orthopyroxene (Fig. A4D). These rocks are dominated by tabular grains of zoned plagioclase (An70-76), prisms and oikocrysts of hypersthene (mg#70-71), and subhedral grains of low-Ca to high-Ca clinopyroxene (mg#75-76). Amphibole and brown phlogopite fill interstices between these cumulate grains. Quartz-orthoclase granophyre, ilmenite, and apatite are also common. Schlieren of granophyre and gabbro-pegmatite are widespread throughout the near-roof zone, commonly cutting across gabbroic units.

Closer to the upper contact, the quartz-pigeonite gabbro becomes texturally more ophitic. The uppermost ~30 m of the YDM are composed of the fine-grained rocks classified as 'upper chilled gabbronorite'; they are more evolved here than at the lower contact.

3.2. Structure of the YDM at the NE and SW margins

3.2.1. The Schkolnyi section

The Schkolnyi section (~1345 m thick; profile II in Fig. 2) represents the northeastern termination of the YDM. Due to limited exposure in this area, this profile is a combined cross-section constructed using samples collected from a number of exploration trenches (up to 200 m long) at the NW slope of Mt. Dovyren, and samples from rocky outcrops at the SE slope of Mt. Dovyren (the upper YDM). The sampling interval along the Schkolnyi section range from 10 to 15 to 20–30 m. Overall, the Schkolnyi section is composed of two rock types: ~2/3 are ultramafics (mostly melanotroctolite) and the remainder includes leucocratic gabbroic rocks (Fig. A5). Based on detailed mineralogy and rock texture (Appendix A, Section A4.1), the Schkolnyi section is subdivided into eight zones, including: (1) lower chilled gabbronorite (~5 m) → (2) plagioperidotite (~100 m) → (3) plagiodunite (~80 m) → (4) intercalation of plagiodunite and melanotroctolite (~350 m) → (5) melano- to mesotroctolite (~390 m) → (6) Ol-containing leucogabbro and gabbro-pegmatite (~230 m) → (7) Ol-free gabbronorite (~110 m) → (8) quartz-pigeonite and granophyre gabbro replaced by the upper chilled gabbronorite at the upper contact (~80 m).

3.2.2. The Yoko section

The Yoko cross-section at the SW termination of the YDM was combined from 32 samples collected along two sub-parallel traverses across the intrusive body (~2200 m thick; see traverses IIIa and IIIb in Fig. 2). Most of the rocks are very fresh and display unaltered original magmatic textures. No single outcrop of the lower YDM contact with hosting rocks was found in this area. However, a gabbronorite dyke ~20–30 m below a suggested contact location (see sample 07DV220-1in Appendix B, Sheet 'Rocks') was proposed to be a compositional proxy of a liquid portion of a parental Ol-laden magma in the YDM area (Ariskin et al., 2015a).

Similar to the Shkolnyi profile, the Yoko section can be divided into mafic and ultramafic parts; however, the relative proportions of these types are very different (Fig. A6 in Appendix A). The amount of Yoko gabbroic rocks is higher, with the first olivine gabbro occurring already within the lower third of the intrusive body. The sampled cross-section starts from a 150 m thick unit of sulphide-bearing plagiodunite, followed by a thick zone of intercalated troctolite and olivine gabbro. At ~1350 m the cumulate succession is dominated by leucogabbro and gabbronorite, similar to the upper intrusion zones in other YDM areas.

There are two distinctive mineralogical features in the Yoko section: 1) unlike other cross-sections, Ol-rich gabbro from Mt. Yoko contains Cr-rich spinel as inclusions in olivine and intercumulus phases; 2) only the uppermost gabbronorite represents Ol-free rocks that are similar to quartz-pigeonite gabbro from other cross-sections of the YDM (sample 07DV230, Appendix B). The most magnesian olivine Fo86 was found in a sulphide-poor plagiodunite from the basal zone of the Yoko section. This composition is similar to the most magnesian olivine from the Schkolnyi area. There is no higher-Fo olivine, as the one documented in the Bolshoi-Tsentralnyi section. This may indicate that both NE and SW parts of the intrusion are composed of crystallisation products of a parental magma that is more evolved than that in the centre of the intrusion.

4. Underlying sills and associated volcanics

In addition to the YDM, the DIC includes a number of mafic-ultramafic sills 10 m to 200 m thick, which are generally sub-parallel to the lower YDM contact (Gurulev, 1965, 1983; Kislov, 1998). Geological mapping has demonstrated that these sills are separated from the bottom of the YDM by beds of hornfels and siltstones. However, some of the bodies may be considered as apophyses from the intrusion (Fig. 2). Numerous dykes of leucocratic gabbronorite and olivine gabbronorite are closely associated with sills, generally cutting both the ultramafic sills and the host rocks (Fig. 10). This mafic-ultramafic association below the YDM seems to be part of a much larger magma plumbing system, which supplied magma to the main Dovyren chamber (Ariskin et al., 2009, 2015a).

4.1. Mafic-ultramafic sills

Similar to the YDM, the underlying sills dip almost vertically, allowing for sampling of their complete cross-sections. Most sills exhibit contrasting layering, which involves leucocratic Ol-bearing gabbronorite, olivine gabbronorite, plagiodunite, and altered peridotite. The gabbroic units appear either as concordant layers up to tens of meters thick, or as cutting dykes (Fig. 10). The largest sampled Camel Sill is located under the central YDM and is ~200 m thick. The lowermost ~55 m of this body is made up of melanocratic olivine-rich gabbronorite, which is chemically similar to the olivine gabbronorite and plagioperidotite from the bottom part of the YDM (see Appendix B, Sheet 'Rocks'; Ariskin et al., 2013b, 2015a). The middle part (~50 m thick) consists of Ol-bearing mesocratic to Ol-free leucocratic gabbronorite, which gives way to overlying plagiodunite (~40 m) and extensively serpentinized peridotite (50 m). The occurrence of the most high-Mg ultramafic rocks above mafic units within this sill, combined with a limited exposure, leaves open the possibility that the Camel Sill represents a combination of separate magma pulses with variable amounts of transported olivine.

4.2. Volcanic sequences

Volcanic rocks of the Synnyr-Dovyren complex include high-Ti basalts of the Inyaptuk suite and overlying low-Ti sequences composed

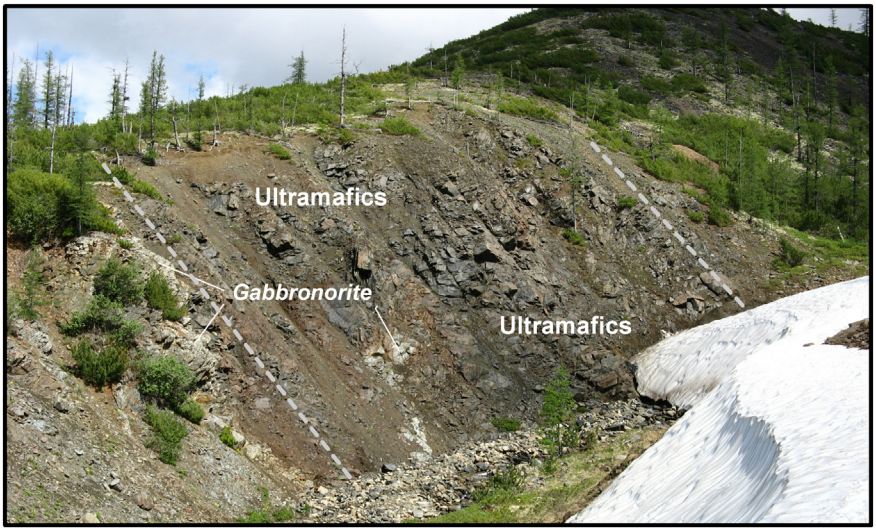

Fig. 10. An ultramafic sill in thermally-metamorphosed sediments below the bottom of the central YDM (Magnetitovyi Creek). Total thickness is ~80 m. Note the occurrence of a more leucocratic gabbronorite dyke, cutting across the sill.

of sills and dykes of gabbrodiabase, siliceous tuffs and basalts, and basaltic andesite (the so-called Synnyr suite described in Kislov, 1998; Fig. 11). The contact between high-Ti and low-Ti suites is demarcated by a horizon of coarse-clastic tectonic breccia (Fig. 11C), which probably formed during tectonic events responsible for the dramatic overturn of the overall volcanic-plutonic sequence. The total thickness of the high-Ti suite is ~250 m (Fig. 2, traverse IVa); however, NE of the intrusion a much thicker sequence of high-Ti massive basaltic flows has been described (Manuilova and Zarubin, 1981; Fig. 11D).

4.2.1. High-Ti basalts and quartz-feldspar porphyry

The high-Ti volcanics of the Inyaptuk suite include subaphyric basalts and, probably, more primitive Cpx-porphyritic basalts (Ariskin et al., 2015a). Due to extensive alteration, the original mineralogy of the subaphyric basalts is inferred from the composition of replacing minerals (chlorite after clinopyroxene) and crystal morphology. In addition, the subaphyric texture involves relics of rare plagioclase phenocrysts (<5%). Their groundmass is dominated by small laths of plagioclase and abundant ilmenite (~10%), reflecting the plagioclase-saturated nature of these basalts. The whole-rock composition of the subaphyric basalts is less magnesian compared to the Cpx-porphyritic basalts (Appendix B, Sheet 'Rocks'). The porphyritic texture of the latter is manifested by abundant (~30%) large (up to 4–5 mm) grains of mostly unaltered clinopyroxene. Rare chlorite pseudomorphs after likely Ol-phenocrysts are also present and locally form intergrowths with clinopyroxene. Some of the porphyritic rocks also contain abundant

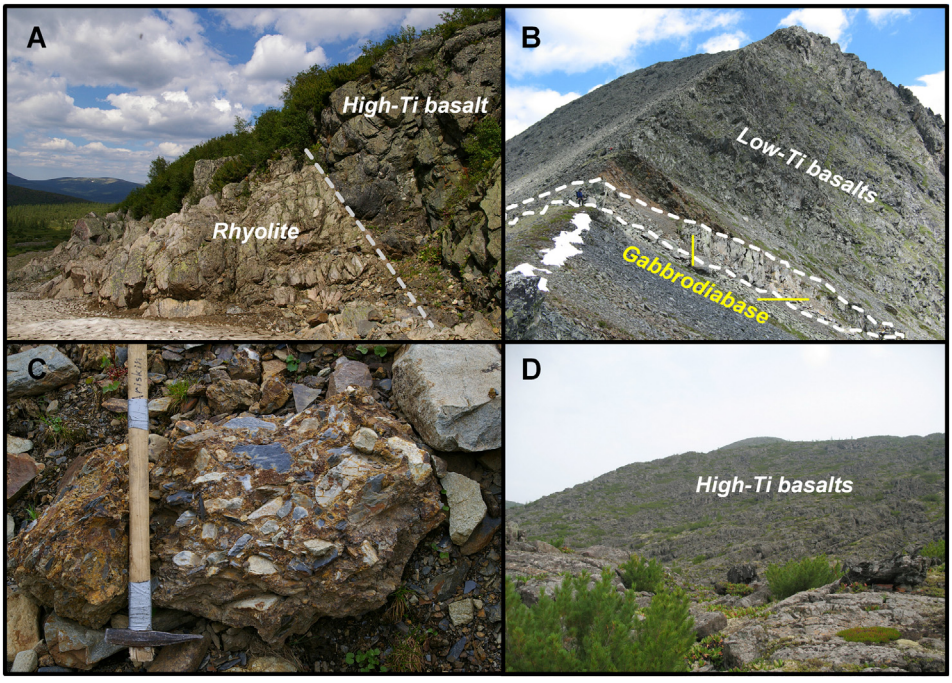

Fig. 11. Volcanic rocks of the Synnyr-Dovyren volcano-plutonic complex. A The contact between a rhyolite dyke and low-Ti basalts of the Inyaptuk suite in the middle stream of Morenny Creek (see traverse IVa in Fig. 2); B The uppermost sill of a gabbro-diabase underlying a sequence of low-Ti basaltic flows, which compose the top of Mt. Soldat at Synnyr Ridge; C A block of a coarse-clastic tectonic breccia from the tectonic boundary between the uppermost high-Ti basalts and overlying volcanic-sedimentary sequence (the Synnyr suite); D A sequence of the high-Ti basalts that compose the widespread basaltic covers NE of the Dovyren area.

sericite pseudomorphs after plagioclase phenocrysts, suggesting that primary mineral assemblages ranged from Ol + Cpx to Cpx + Ol + Pl.

Another important feature of the Inyaptuk suite is the presence of quartz-feldspar rhyolite dykes (up to 50 m thick), which cut sedimentary rocks and basalt flows near the bottom of the volcanic succession (Fig. 11A). These are leucocratic porphyritic rocks with a microspherulitic felsic groundmass including accessory titanomagnetite. Relic phenocrysts of quartz and plagioclase make up 10–15 vol% of the rock. Quartz phenocrysts have mostly ovoid shape and are generally overgrown by a microcrystalline quartz-feldspar aggregate. The rocks contain abundant grains of zircon, which were used to date the felsic volcanics and the timing of overprinting processes.

4.2.2. Low-Ti volcanics

The low-Ti Synnyr (sub)volcanic suite includes meso- to leucocratic gabbrodiabase and gabbronorite forming several meters thick bodies on the SW slopes of the Synnyr Ridge and basalt to basaltic andesite flows both along the ridge crest and on the NE slopes of Synnyr Ridge (Figs. 2 and 11B). The largest (~200 m thick) sill concordant with hosting volcano-sedimentary rocks was sampled at the SW slope of Mt. Soldat (summit 2232 m in Fig. 2; Ariskin et al., 2015a). It is composed of fine-grained granophyric gabbronorite with a relict gabbroophitic texture. Similar to other subvolcanic rocks, it consists of completely saussuritized lath-like plagioclase and uralitized pyroxene. The original orthopyroxene is replaced by secondary chlorite, whereas clinopyroxene is replaced by actinolite. The interstices between the relic plagioclase and pyroxene crystals contain subgraphic quartz-albite intergrowths. Ilmenite plates are also common. The predominant accessory minerals include Cu-Fe sulphides, titanite, and rutile.

Subaphyric and aphyric basaltic andesites were sampled among low-Ti flows at the summit of Mt. Soldat. These are massive rocks with a relic micro-intersertus texture defined by microlites of saussuritized plagioclase and amphibolized pyroxene. There are also finely dispersed sulphides, including both pentlandite and Ni-bearing pyrrhotite, and rutile. The whole-rock compositions of the low-Ti volcanics are generally similar to the chilled gabbronorite from the roof and bottom of the YDM in the Schkolnyi section, and mafic dykes below the lower contact of the YDM in the Schkolnyi and Yoko areas (compare the gabbrodiabase 07DV183-1 and the basaltic andesite 07DV192-1 with samples S25-1 to S25-6 or 07DV220-1 in Appendix B). As discussed below, the low-Ti volcanics are likely related to the YDM (Ariskin et al., 2015a).

5. Trace element geochemistry

Concentrations of incompatible elements in most intrusive rocks and representative volcanics of the Synnyr-Dovyren Complex are given in Appendix B (Sheet 'Rocks') and partly published by Ariskin et al. (2015a). These data are summarised on mantle-normalised diagrams (Fig. 12). Overall, the compositions of the YDM rocks have broadly similar mantle-normalised spectra, best seen in similar variations of REE, LILE, and HFSE, including a distinct Nb-Ta minimum and a minor depletion in Zr and Ti, and high enrichment in Pb. A more detailed comparison reveals some differences in whole rock geochemistry between the Bolshoi-Tsentralnyi and Schkolnyi cross-sections.

5.1.1. The centre of the YDM

Geochemical spectra of the chilled rocks and plagioperidotite in Fig. 12A represent samples from both 'Fo88' and 'Fo86-trends' trends (Fig. 8B). All the near-contact rocks are geochemically similar, with only subtle variations of incompatible element concentrations due to minor magma fractionation, consistent with the narrow compositional range of melts in equilibrium with olivine Fo88 to Fo86. These rocks are also similar to the fine-grained olivine gabbronorite near the lower contact of the Camel Sill (sample DV35-2; Appendix B, Sheet 'Rocks'). The plagiodunite is more depleted in incompatible elements compared to the YDM contact rocks. All patterns for dunite, troctolite, and olivine gabbro are characterised by very low concentrations of incompatible elements (Fig. 12B, C and D). The lowest concentrations of incompatible elements are typical for the troctolite. The geochemical patterns are

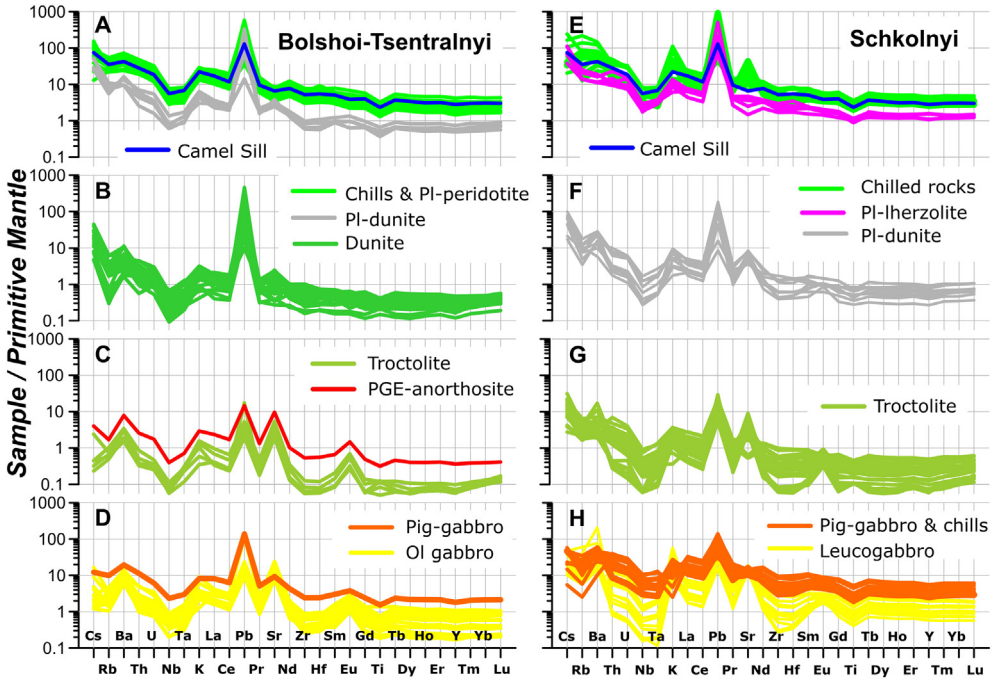

Fig. 12. Mantle-normalised incompatible trace element contents of samples from the YDM and the underlying sills. Plots A to D show samples from the Bolshoi-Tsentralnyi cross-section: A Chilled rocks, plagioperidotite and plagiodunite; B Dunite zone; C Troctolite; D Gabbroic rocks. Plots E to H show samples from the Shkolnyi cross-section: E Basal chilled rocks and plagioperodotite; F Plagiodunite; G Troctolite; H Upper chilled rocks. The composition of an endocontact rock from the Camel Sill is shown in plots A and E for comparison. All compositions were normalised to a primitive mantle from Sun and McDonough (1989).

consistent with petrographic observations indicating an inward decrease in the porosity of olivine and olivine-plagioclase cumulates, which is a measure of the amount of the intercumulus melt.

5.1.2. The Schkolnyi section

Geochemical patterns of rocks from the NE termination of the YDM resemble those in the centre of the intrusion. Maximum concentrations of incompatible elements are typical for chilled gabbronorite and plagioperidotite from the lower contact zone, and quartz-pigeonite gabbro to chilled gabbronorite from the roof (Fig. 12E, H). The quartz-pigeonite gabbro has higher concentrations of REE and slightly lower abundances of LILE and Sr compared to the chilled rocks from the bottom. Most samples of melanotroctolite and many olivine gabbro samples display the lowest incompatible element concentrations (Fig. 12G, H). Unlike the Bolshoi-Tsentralnyi cross-section, plagioperidotite from the Schkolnyi Section is readily distinguished from the chilled rocks due to depletion in incompatible elements (Fig. 12E). Another difference from the centre is the presence of positive anomalies of K and Sr in chilled rocks and plagiodunite (compare Figs. 12 A, B and E, F). Overall, the entire succession of mafic to ultramafic rocks from the Schkolnyi Section displays higher concentrations of incompatible elements than in the central YDM. This is additional evidence for a more-evolved composition of the parental magma intruded in the NE margin of the YDM chamber.

5.1.3. Low-Ti and high-Ti volcanics

Ariskin et al. (2015a) have demonstrated that the geochemical spectrum of the low-Ti basalts of the Synnyr suite is similar to that of the YDM chilled rocks, gabbro and gabbronorite. The data shown in Fig. 13A support the hypothesis that Synnyr volcanics are likely comagmatic with YDM magmas, particularly the Schkolnyi upper contact rocks, even though the Nb-Ta minimum in the Synnyr gabbro-diabase and basaltic andesite is not as pronounced as in the YDM contact facies. Compared to the low-Ti volcanics, the high-Ti basalts of the Inyaptuk suite display different mantle-normalised patterns, which lack both Nb-Ta and Sr minima (Fig. 13B). This is consistent with the Sr-Nd isotopic differences shown in Fig. 4.

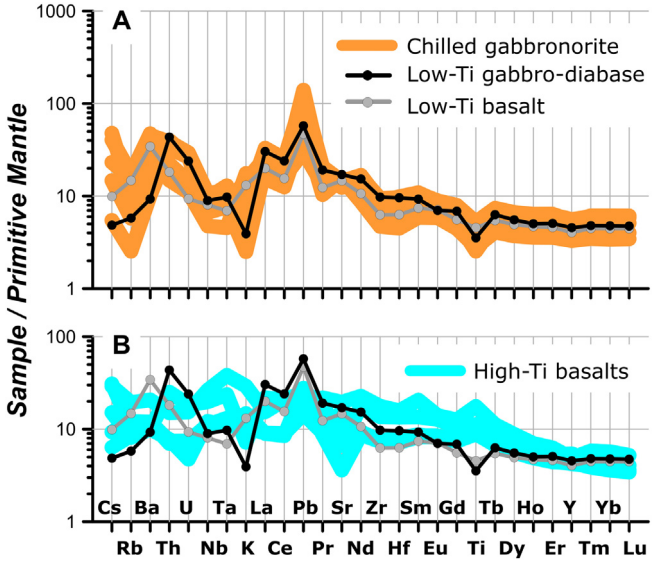

Fig. 13. Mantle-normalised patterns of incompatible elements in low-Ti volcanics compared to characteristics of the roof gabbronorite from the YDM and high-Ti basalts. The low-Ti compositions in both plots represent the Synnyr gabbro-diabase 07DV183-1 and basaltic andesite 07DV192-1, including comparisons: A Uppermost gabbronorite from the Schkolnyi Section; B High-Ti basalts 07DV323-1, 327-6, 327-7, and AA30 (see compositions in Appendix B, Sheet 'Rocks'). Normalisation to a primitive mantle from Sun and McDonough (1989).

6. Discussion

In this section, we focus on modelled characteristics of the Dovyren parental magmas and possible formation mechanisms of the layered YDM structure. The cumulate succession is shown to be related to the history of sulphide saturation in the Dovyren magma chamber. Finally, a probable mantle source of the Dovyren magmas is discussed.

6.1. Parental magmas of the Dovyren Intrusive Complex

Ariskin et al. (2003) presented probable parameters of the Dovyren magma based on COMAGMAT modelling of equilibrium crystallisation for 10 ultramafic compositions, which represent the bottom of the intrusion and the underlying sills. As a result, a sub-eutectic parental magma (Ol + Pl ± pyroxene) was proposed, which had a temperature of 1180–1190 °C and contained ~40% of transported olivine. The modelled melt contained ~54 wt% SiO_2 and ~7.5 wt% MgO, being in equilibrium with olivine Fo84.6 and plagioclase An80.5 (Table 1). However, Bolikhovskaya et al. (2007) pointed out that the dunite zone of the YDM does not contain any record of cotectic Ol-Pl crystallisation. Instead, intercumulus plagioclase in dunite is much less anorthitic than that in the overlying troctolite (Fig. 9). Further studies of the lower contact zone indicated that most contact rocks should be interpreted as originally Ol-rich cumulates, crystallised from a magnesian parental magma in equilibrium with olivine ~Fo87 (Ariskin et al., 2009). In this case, the COMAGMAT calculations predict that upon emplacement the original magmatic melt would contain 9–10% wt% MgO at ~1240–1270 °C.

Based on the FeO vs. MgO relationships for the basal YDM ultramafics (Fig. 8B), it is possible to calculate probable parental magma compositions more accurately (Ariskin et al., 2016). As mentioned above, there are two distinct petrochemical trends: the Fo88-trend includes all samples of chilled gabbronorite to picrodolerite and a continuum of plagioperidotite to plagiodunite, whereas the Fo86-trend is formed by the rest of the plagioperidotite and plagiodunite compositions (Fig. 8B). Since both groups of rocks occur in the same cumulate succession, we interpret these observations as evidence for the early stages of YDM formation, including almost coeval emplacement of a compositional range of olivine-laden magmas carrying variable amounts of intratelluric olivine Fo86 to Fo88.

To estimate an initial temperature of the most primitive magma (Fo88 + melt), one can utilize the results of COMAGMAT-5 calculations simulating equilibrium crystallisation of the primitive DV30-2 picrodolerite sampled ~1.4 m above the lower contact of the YDM within the chilled zone (Ariskin et al., 2016; Table 1). This is because the composition of this rock belongs to the Fo88-trend in Fig. 8B. As follows from data in Table 1, the equilibrium state of a modelled mixture of 37.4 wt% olivine Fo88 and 62.6 wt% magmatic melt is consistent with the 1285.4 °C equilibrium temperature. The modelled initial melt contains ~11 wt% MgO; this is very similar to the composition of a chilled gabbronorite sampled at a 10 cm distance from the lower contact (see 'CGN' column in Table 1).

The results of this modelling characterise compositions of two most primitive phases of the Dovyren magma, whereas, the calculated value 37.4 wt% olivine is attributed to a primitive olivine orthocumulate containing relatively large amounts of intercumulus melt. The contact cumulate is assumed to crystallise at the same initial temperature as a parental magma composed of the same magmatic melt and unknown amount of olivine Fo88. Assuming that sorting and accumulation of olivine suspended in the parent melt could affect the bulk composition of cumulus mixtures during their solidification near the lower contact, one can state that the amount of olivine in the parental magma could not exceed 37%. This is an upper limit, which is consistent with the bulk MgO composition that is below 24 wt%. At this stage, we cannot provide accurate estimates of the modal and chemical composition of the most primitive Dovyren magma. However, the occurrence of chilled

Table 1
Primitive chills and parameters of parental magmas proposed for the Dovyren Intrusive Complex.

Melt components, wt%	This study					Ariskin et al. (2003), n = 10	
	CGN	DV30-2	DV30-2 melts		07DV220-1	1185 °C	S.D.
			1285.4 °C	1189.7 °C			
SiO_2	53.20	47.51	52.14	54.27	53.14	54.13	0.80
TiO_2	0.65	0.39	0.63	0.74	0.61	0.78	0.10
Al_2O_3	14.15	8.79	14.12	15.34	15.52	15.24	0.42
Fe_2O_3	–	–	0.86	0.84	–	–	
FeO	9.38	9.83	8.16	6.62	7.98	8.19	0.57
MnO	0.22	0.17	0.16	0.14	0.15	0.15	0.02
MgO	10.64	24.42	10.94	7.62	8.12	7.51	0.33
CaO	9.31	6.34	10.00	11.05	10.99	11.33	0.87
Na_2O	1.28	1.08	1.74	1.97	1.94	1.65	0.47
K_2O	0.79	0.62	1.00	1.17	1.26	0.88	0.25
P_2O_5	0.11	0.08	0.13	0.16	0.12	0.14	0.09
Cr_2O_3	0.10	0.57	–	–	0.08	–	–
NiO	0.032	0.142	0.034	0.017	0.015	–	–
S	0.13	0.05	0.080	0.065	0.07	–	–
SCSS	–	–	0.099	0.065	–	–	–
Modelled characteristics of the proposed magmas							
Ol, wt%	–	–	37.4	44.8	–	–	–
Pl, wt%	–	–	–	2.1	–	–	–
Sulphide, wt%	–	–	–	0.044	–	–	–
Fo, mole%	–	–	88	86	–	84.6	±1.0
An, mole%	–	–	–	78.6	–	80.5	±4.5

CGN and DV30-2 are chilled gabbronorite (07DV100-3b-I) and picrodolerite sampled at the distance of 10 cm and 1.4 m from the direct contact with contact hornfels; 07DV220-1 represents a comagmatic gabbro-diabase dyke below the lower contact of the YDM in the Yoko area (Appendix B). Columns '1285.4 °C' and '1189.7 °C' are melt compositions calculated at 1285.4 °C and 1189.7 °C, as a result of modelling equilibrium crystallisation of DV30-2 using the COMAGMAT-5 program (Ariskin et al., 2013a). The '1185 °C' composition is an initial magmatic melt calculated for 10 samples of plagioperidotite (mostly from sills) using COMAGMAT-3.5 (Ariskin et al., 2003). S.D. is standard deviation (1σ).

rocks and rare dykes of 17–20 wt% MgO (see picrodolerites DV30-1, 07DV100-1, and dyke T1-7 in Appendix B) reflects a probable picritic parental melt.

Further crystallisation of the DV30-2 cumulate system generates more-evolved melts. As the temperature decreases to 1189.7 °C, the equilibrium state corresponds to a cotectic mixture of 44.8 wt% olivine Fo86, 2.1 wt% plagioclase An78.6, a small amount of Fe-Ni sulphide liquid, in equilibrium with a melt containing ~7.6 wt% MgO. The melt composition closely resembles that of the 07DV220-1 gabbro-diabase, sampled below the lower YDM contact in the Yoko area (Table 1). The calculated melt is also similar to the 'original YDM melt' calculated by Ariskin et al. (2003), despite the fact that the authors utilized other ultramafic compositions and another magma crystallisation model (COMAGMAT-3.5) instead of the COMAGMAT-5.2 used in this study.

We suggest that the modelled melt composition, given as the '1189.7 °C' column in Table 1, may be considered to be a close approximation of the magmatic parental melt consistent with olivine Fo86 in the more-evolved Ol-laden Dovyren magma (Fig. 8B). Thus, this modelling resolves the apparent contradiction between the first COMAGMAT-3.5 calculations and the present cumulate structure of the YDM centre (Bolikhovskaya et al., 2007). The earliest estimate of the Dovyren magma (Ariskin et al., 2003) should be treated now as recovering the second relatively-evolved intrusion-forming magmatic melt.

Overall, the results suggest a diversity of olivine-laden to multiply-saturated magmas, which formed the YDM. The most primitive and higher-temperature magma was saturated with olivine (+spinel), whereas its lower temperature derivatives represent Ol-Pl cotectics. Based on the structure of the YDM (Figs. 5 and 9), it is possible to suggest that the central part of the intrusion was formed predominantly by high temperature 'Fo88-magma', whereas its peripheral zones and ultramafic apophyses crystallised from the lower temperature 'Fo86-magma'. This inference is supported by the presence of a large volume of dunite in the centre, which is absent in the Schkolnyi and Yoko sections, and by the presence of less magnesian olivine compositions observed within the cross-sections in the marginal areas (Figs. 5, 9 and A5/A6 in Appendix A). Some of the mafic-to-ultramafic sills beneath the main intrusive body might be formed by even more evolved Ol + Pl-saturated magmas; however, this hypothesis needs further investigation.

6.2. Sulphide immiscibility in the proposed magmas

Understanding the sulphide saturation history of mafic-to-ultramafic igneous systems includes responding to the question: 'Is the amount of magmatic sulphur sufficient for reaching sulphide immiscibility at early stages of magma evolution'? Ripley and Li (2013) have considered how sulphur capacity varies in open and closed magmatic systems evolving by fractional crystallisation. They emphasised that in open magma conduits, where efficient sequestration of sulphide from a large magma volume is possible, an external source of sulphur may not be required to form magmatic sulphide mineralisation. Conversely, in closed magma chambers, sizeable sulphide-rich magmatic mineralisation is unlikely to form without assimilation of sulphur from the host rocks, because 20 to 40% magma crystallisation is required before the onset of sulphide immiscibility, with the consequent sequestration of nickel and other metals of interest in the early forming silicate phases. However, they also concluded that mantle-derived magmas crystallised as closed systems have the more likely potential to generate Cu and PGE sulphide-poor reefs.

Sulphide mineralisation in the YDM and the compositions of the proposed parental magmas provide insights into sulphide saturation processes in mafic systems. Comparing the modelled S concentrations with estimates of sulphide solubility in melts from our area of interest (Table 1), it is possible to quantify the onset of sulphide immiscibility in the crystallising DV30-2 cumulate. At the initial temperature of 1285.4 °C the S concentration is 20% lower than SCSS, reflecting the sulphide-unsaturated character of the most primitive Dovyren magma. At the temperature of 1189.7 °C the COMAGMAT-5 modelling predicts 650 ppm S = SCSS in the melt. This is consistent with sulphide-saturated conditions and the occurrence of ~0.04 wt% sulphide among crystallising olivine and plagioclase (Table 1). In fact, sulphide

immiscibility in the DV30-2 system started at $T \sim 1248$ °C, i.e. 30–40 °C below the magma emplacement temperature in equilibrium with olivine ~Fo87 (Ariskin et al., 2016).

These results suggest that the olivine cumulate piles in the centre of the YDM attained sulphide immiscibility during crystallisation of the intercumulus melt at a post-cumulus stage. As a result, a Ni-rich immiscible sulphide liquid is assumed to have originated directly in the cumulate pile, followed by its downwards migration to form a poorly-mineralised plagiodunite horizon (Ariskin et al., 2016). This conclusion is supported by field observations and chemical rock analyses, which indicate that a number of basal cumulates are oversaturated with sulphides in the intercumulus melt, particularly within plagiodunite and plagioperidotite.

To explain such a local enrichment (which could not be generated in situ due to the very low 'crystallisation' proportion of sulphides), one should suggest a downward transport of the immiscible sulphide liquid and its concentration within the cumulate piles. On the contrary, less primitive cumulates from the Schkolnyi and Yoko sections crystallised from sulphide-saturated magmatic melts. The modelling-based conclusions may explain the absence of essential sulphide accumulation in the most primitive ultramafic rocks from the central YDM and a widespread distribution of Cu-Ni sulphide ores in the NE and SW terminations of the intrusion. This is also consistent with the occurrence of patchy to net-textured Cu-Ni sulphide ores in relatively evolved olivine gabbronorite, exposed as dykes and sills along and underneath the lower YDM contact (Ariskin et al., 2016; Kislov, 1998).

In addition, the results of the sulphide immiscibility calculations are consistent with the conclusion of Ripley and Li (2013) that mantle-derived magmas have the potential to generate Cu-sulphide-rich PGE reefs in closed magma systems. In fact, even small portions of the intercumulus sulphide liquid can extract most PGE and other highly-chalcophile elements from the melt (Mungall and Brenan, 2014). We suggest that in the troctolite and gabbroic parts of the Dovyren chamber, sulphide immiscibility occurred at the temperatures around 1200 °C, generating Cu-rich sulphides, which formed the sulphide-poor PGE-rich troctolite and PGE-rich anorthosite (Figs. 5 and 7). However, we argue that PGE-rich sulphide-poor mineralisation in the YDM troctolite and anorthosite formed in the Dovyren magma chamber as it evolved as an open system, at least in the initial to middle stages of its evolution.

6.3. Fingerprints of an open magma chamber

Following from geochemical data on chilled rocks from the lower contact, the modelled porosity of olivine ± plagioclase cumulates, and a narrow range of mineral compositions throughout the YDM, Ariskin et al. (2003) have concluded that there was no large-scale magma fractionation in the Dovyren chamber. Instead, they suggested that the main formation mechanism of the contrasting YDM structure was the compaction of the original olivine-rich cumulate piles, accompanied by upward migration of the intercumulus melt through the porous space of partly-crystallised cumulates. However, it is unclear whether these melts accumulate and crystallise in the upper part of the magma chamber, or whether they migrate out of the heterogeneous magmatic reservoir, leaving behind a crystalline residue of low-porosity ultramafic and gabbroic cumulates. In the first case, one can argue for a closed magma chamber, with the average intrusion composition consistent with that of the basal picrodolerite/plagioperidotite. The second scenario suggests the depleted character of the average weighted composition of the Dovyren intrusion compared to that of the contact rocks as a proxy for the composition of probable parental melts. Such misbalance should first be reflected in the concentrations of components partitioning into the melt, including incompatible major and trace elements.

6.3.1. Misbalance of incompatible components

Fig. 14 presents variations in SiO_2, TiO_2, and four trace elements in the Dovyren rocks along cross-sections in the central part of the intrusion and in the Schkolnyi area. Zr, Y, and Nb were selected as incompatible elements; they are relatively immobile at the secondary alteration. Rb is chosen to assess the behavior of potentially mobile elements. Rocks from both sampled cross-sections display a C-shaped chemostratigraphy, with elevated whole rock concentrations being towards the lower and upper contacts, and a marked depletion within the inner parts of the intrusion. The maximum incompatible element concentrations of the lower contact picrodolerite are very similar to those observed in olivine gabbronorite from ultramafic sills and associated dykes. This supports previous interpretations that the contact YDM rocks approximate the parental magma composition (Ariskin et al., 2009). Overall, these geochemical patterns illustrate the ultra-depleted character of the intrusion, because the dunite, troctolite, and most of the gabbroic rocks are 3–5 fold depleted in incompatible elements as compared to the contact facies, particularly chilled gabbronorite.

The calculated weighted average compositions of the YDM are listed in Table 2. Columns 1–3 represent published estimates for the major rock-forming elements (Bolikhovskaya et al., 2007; Konnikov, 1986; Yaroshevskii et al., 1982). The values in columns 4 ('Aver-1') and 7 ('Aver-2') for the Bolshoi-Tsentralnyi and Schkolnyi sections, respectively, are based on major element and trace element analytical data summarised in this study (Appendix B, Sheet 'Rocks'). Thus, our estimates from this work are consistent with the ones from previous studies, indicating a high-MgO YDM composition: ~27–29 wt% MgO and around 44 wt% SiO_2. Due to somewhat elevated Al_2O_3 (~10 wt%) at present MgO, it could be treated as a 'troctolite-like' composition (Ariskin et al., 2009). Comparison of data given in columns 4 and 7 evidences a slightly more magnesian composition at the centre of the intrusion than that at the NE termination. This is consistent with the absence of adcumulate dunite in the Schkolnyi section (Fig. A5 in Appendix A) and the above conclusion that the marginal parts of the intrusion were formed during crystallisation of a lower temperature, more evolved magma (Table 1). This inference is also supported by higher concentrations of TiO_2, K_2O, P_2O_5, and other incompatible elements in the Schkolnyi Section (Fig. 14B; Appendix B, Sheet 'Rocks').

In addition, Table 2 includes two compositions denoted as 'Proxy-1' and 'Proxy-2' in columns 4 and 8, respectively. These compositions are considered to be a close approximation of olivine-laden Dovyren magmas, assuming that those should have MgO and mg# similar to the weighted average YDM compositions (following from a 'closed magma chamber' scenario). Proxy-1 represents the 07DV132-3 plagioperidotite from the bottom zone of the YDM, which belongs to the Fo88-trend in Fig. 8B. Proxy-2 corresponds to a mixture of 68.8% olivine gabbronorite T1-7 (from a dyke sampled 50 m underneath the lower contact of the YDM in the Schkolnyi area) and 31.2% olivine Fo86. Both sample compositions are listed in Appendix B (Sheet 'Rocks'). Columns 6 and 9, denoted as 'Av/Pr', represent ratios of the 'Aver-1' and 'Aver-2' concentrations to those of the two proxies above. These calculations indicate that both average YDM compositions are 2–5 fold depleted with respect to the proposed Dovyren magmas, with the cross-section in the centre being more depleted than that in the Schkolnyi area. The depleted character of the YDM suggests that at least ~50 to 70% of intercumulus gabbronorite melts were expelled from the magma chamber during chamber formation and solidification.

6.3.2. Significance of the Al_2O_3-SiO_2-MgO diagram

Additional evidence for the open magma chamber is given in Fig. 15, which presents a projection of the YDM whole-rock compositions onto the Al_2O_3-SiO_2-MgO plane. There are two well-defined trends in the ternary diagram, which yield insight into the origin of the Dovyren rocks. The first trend represents nearly concurrent tie-lines between observed olivine compositions (Fo84-88) and a chilled YDM facies, displaying a linear sequence of picrodolerite, plagioperidotite, plagiodunite, and the lowest dunite. Figurative points of these rocks are located in the order of decreasing olivine cumulate porosity, so that more magnesian rocks contain less intercumulus. One can suggest that the maximum

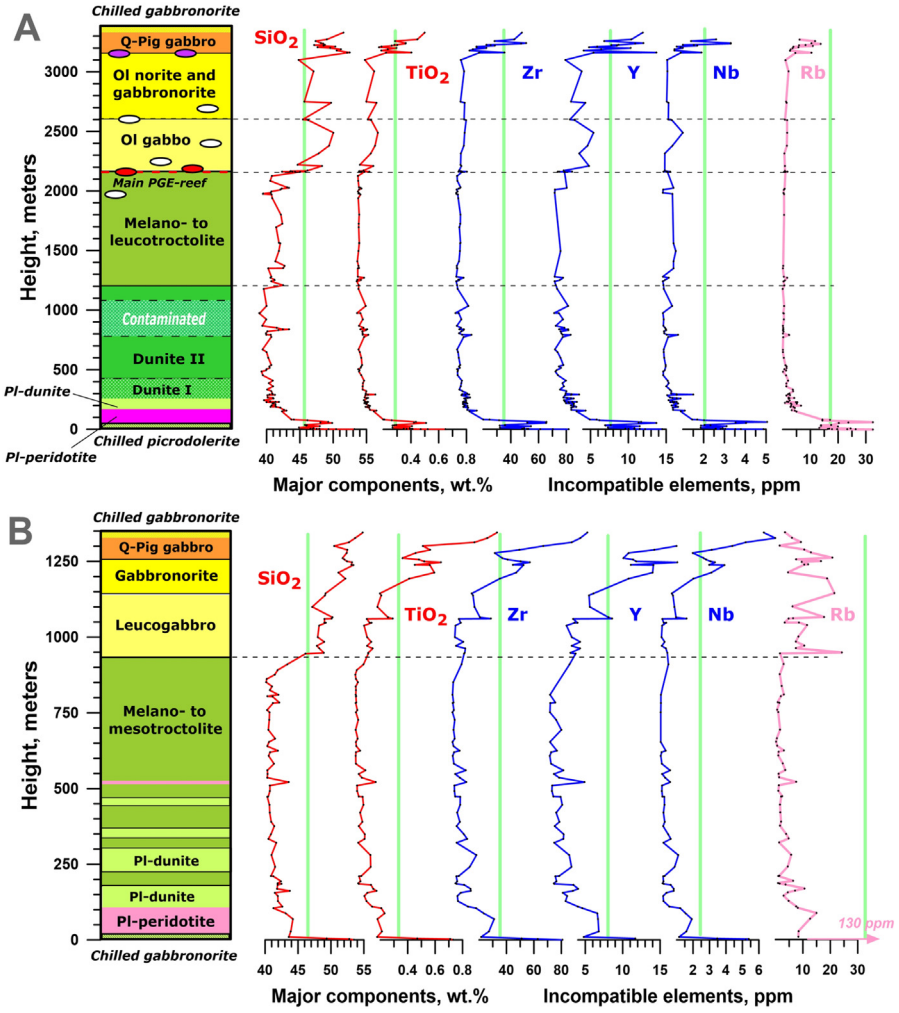

Fig. 14. Chemostratigraphy of SiO_2, TiO_2, and selected trace elements in the YDM. Cross-sections of the YDM: A Bolshoi-Tsentralnyi; B Schkolnyi. The green lines represent two approximations of olivine-rich parental magmas from Table 2: A Proxy-1, B Proxy-2.

porosity is recorded in the composition of the chilled gabbronorite, which has the lowest MgO due to a minimum amount of suspended olivine (Fig. 15). Such linear compositional relationships are typical only for a basal zone ~250 m thick (Figs. 5 and 9).

Another distinct trend includes a diversity of the Dovyren troctolite (Fig. 15), with whole-rock compositions following a tie-line connecting those of pure olivine and plagioclase (An84-87). This observation argues that the Dovyren troctolite should be considered as a binary adcumulate mixture of olivine and plagioclase (plus traces of spinel), which is almost free of Px-containing intercumulus material. The same conclusion is true for the adcumulate dunite, because the compositions of rocks from the dunite zone fall close to pure olivine in the ternary diagram (Fig. 15). These distinct trends support the inference that the original characteristics of the olivine-laden magmas are recorded in the variable ultramafic compositions from the basal zone, whereas the adcumulate nature of dunite and troctolite reflects a large-scale expulsion of intercumulus melt from the magma chamber. Whole-rock compositions, which fall in between two major trends, represent cumulate gabbroic and anorthositic rocks from the upper YDM.

Assuming the open character of the Dovyren magma chamber, it is possible to explain the unusual 'troctolite-like' weighted average compositions of the YDM rocks (Table 2). We have demonstrated that the YDM parental magmas were saturated in olivine + spinel and carried a variable but substantial amount of olivine crystals. However, the average YDM composition (Table 2) plots away from the initial olivine – melt tie-line, which connects the original olivine composition (~Fo88) and probable magmatic melt (Fig. 15). This shift towards the olivine-plagioclase tie-line (i.e., a lower SiO_2 and higher Al_2O_3 as compared to the olivine – melt trend) is direct evidence for the loss of a significant amount of primitive and residual melts from the Dovyren magma chamber, giving rise to the increased proportion of olivine and plagioclase in the average 'troctolite-like' YDM composition.

6.4. Formation and evolution of the Dovyren magma chamber

In addition to the 'compaction hypothesis' discussed above, it is possible to speculate whether the observed large-scale depletion in incompatible elements may be due to a magma-staging system that evolved in the upper part of the Dovyren magma chamber, where large amounts of olivine gabbronorite magmas passed through leaving behind cumulate piles as a melt-depleted precursor of Ol-rich to gabbroic adcumulates. The proposed mechanism is similar to the one that explains the origin of olivine-plagioclase adcumulus aggregates (the so-called 'allivalites') found as xenoliths in volcanic systems of the Kamchatka Peninsula in Russia (Plechov et al., 2008). Both scenarios are important for the development of a petrologic-geological model of the formation and evolution of the Dovyren magma chamber. Below, we propose such hybrid mechanism, including four stages whereby magma emplacement and early crystal sedimentation proceeded simultaneously, followed by the formation of adcumulates during compaction and in situ crystallisation of the original cumulate piles.

Table 2
Average weighted compositions and proposed proxies of the most primitive olivine orthocumulates of the Yoko-Dovyren massif.

Oxide, wt%	Previous studies			Bolshoi-Tsentralnyi section, n = 141			Schkolnyi section, n = 89		
	1	2	3	4	5	6	7	8	9
	n = 256	–	n = 114	Aver-1	Proxy-1	Av/Pr	Aver-2	Proxy-2	Av/Pr
SiO_2	44.54	45.00	43.92	43.87	45.82	0.957	44.18	46.41	0.952
TiO_2	0.09	0.21	0.11	0.10	0.29	0.354	0.16	0.32	0.503
Al_2O_3	10.64	10.27	9.72	9.74	7.31	1.334	10.12	7.66	1.321
FeO	10.05	10.95	10.53	9.94	10.36	0.959	10.31	11.09	0.930
MnO	0.14	–	0.17	0.16	0.17	0.932	0.17	0.18	0.927
MgO	26.57	24.31	27.88	**28.50**	**29.23**	0.975	**26.98**	**26.94**	1.001
CaO	7.35	6.87	6.99	6.66	5.06	1.314	6.73	5.88	1.145
Na_2O	0.54	0.78	0.59	0.59	0.48	1.217	0.78	0.54	1.430
K_2O	0.07	0.28	0.07	0.12	0.52	0.225	0.24	0.82	0.294
P_2O_5	0.01	–	0.02	0.02	0.06	0.292	0.03	0.06	0.512
Cr_2O_3	–	–	–	0.31	0.69	0.441	0.31	0.10	3.173
mg#	0.825	0.805	0.825	0.836	0.834	–	0.824	0.812	–
S, wt%	–	–	–	0.055	–	–	0.085	–	–
Trace elements, ppm									
Zr				9.37	35.8	0.262	14.5	34.71	0.417
Y				2.32	7.69	0.302	4.20	7.98	0.527
Nb				0.485	2.04	0.237	0.863	2.37	0.365
Rb				2.24	17.5	0.128	6.45	33.4	0.193
Ba				50.3	228	0.221	123	217	0.567
Sr				95.7	85.6	1.118	140.8	77.1	1.828
Sc				11.9	21.8	0.546	18.0	18.6	0.966
V				42.9	106	0.404	81.9	123.3	0.664
La				1.23	7.42	0.166	2.86	5.83	0.490
Eu				0.104	0.424	0.245	0.255	0.385	0.664
Lu				0.027	0.121	0.222	0.069	0.147	0.466

The average YDM compositions are normalised to a volatile-free basis. Previous studies: 1 Yaroshevskii et al. (1982), calculated as the average of 256 rocks sampled through the entire massif; 2 Konnikov (1986); 3 Bolikhovskaya et al. (2007), calculated for a combined cross-section 2950 m thick. Assumed original olivine cumulates (slightly enriched in olivine with respect to a probable olivine-laden (picritic) parental magma: Proxy-1 is plagioperidotite 07DV132-3 from the bottom zone of the YDM in the centre (the "Fo88"-group in Fig. 8B); Proxy-2 corresponds to a mixture of 68.8% olivine gabbronorite T1-7 and 31.2% olivine Fo86. The whole-rock compositions are given in Appendix B (Sheet 'Rocks'). Ratios emphasised using black colour in columns 6 and 9 demonstrate a relative enrichment of the average YDM in 'plagioclase-elements', such as Al, Ca, Na, and Sr.

6.4.1. The first stage

The formation of the Dovyren chamber may be considered as a result of numerous pulses of olivine-laden geochemically similar picritic magmas (17–20 wt% MgO), spanning a temperature range of 100 °C, approximately from 1290 °C (Fo88) to 1190 °C (Fo86). The magma emplacement process was fast enough to escape complete solidification of each pulse, thus accommodating the continued growth of the magma chamber. Large-scale sedimentation of the olivine crystals started simultaneously with the filling and growth of the magma chamber, thus giving rise to an original Ol-rich cumulate pile and an overlying layer of crystal-depleted gabbronoritic magma. The uppermost mafic part of the growing Dovyren chamber was not stagnant; it evolved as an open magma flowing system. Occurrence of autoliths of plagiolherzolite in the upper part of the YDM (D.A. Orsoev, *pers. comm*) may be considered as a record of the first stage process.

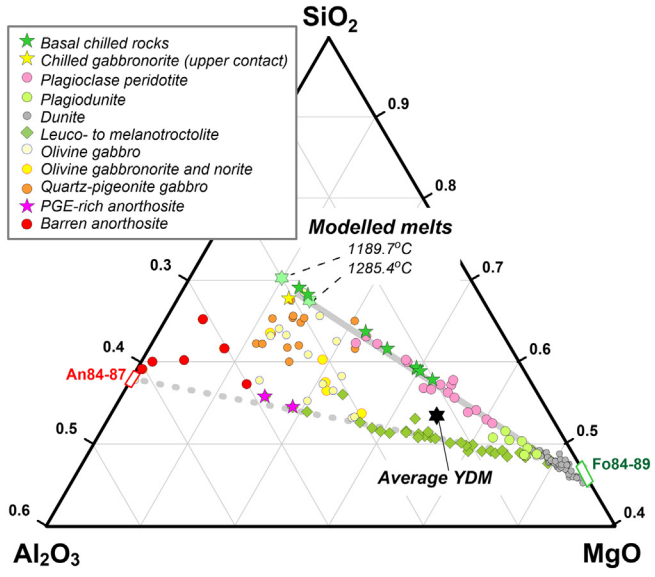

Fig. 15. The Al_2O_3-SiO_2-MgO diagram for the whole-rock compositions from the central YDM (the Bolshoi-Tsentralnyi section). Modelled melts represent two compositions calculated at 1285.4 and 1189.7 °C (see Table 1 and Fig. 8B). The average YDM composition is given in Table 2 as 'Aver-1'.

During chamber formation, assimilation of the country rocks could take place; however, we still cannot evaluate this process quantitatively. Preliminary estimates from isotope studies suggest that this interaction had minor effect on the bulk magma composition (Ariskin et al., 2015a). It is also unclear whether carbonates acted as the country rock that hosted the original (much smaller) magma chamber. It is only possible to suggest that the carbonate horizons collapsed and partly dissolved during the later stages of the magma chamber formation (Wenzel et al., 2002), accommodating the continuing growth of the magma chamber accompanied by the proposed large-scale differentiation. The undisturbed structure of the marginal part of the YDM in the Schkolnyi area, where carbonate xenoliths are absent, supports this inference (Fig. 14B).

6.4.2. The second stage

At the time when the magma chamber attained its final size and geometry, it had already developed a layered heterogeneous structure, with most olivine crystals accumulated in its lower 'ultramafic' part, promoting the formation of a relatively crystal-depleted non-stagnant upper 'gabbroic' part. After a critical mass of olivine cumulates formed, compaction of the cumulate pile started, accompanied by additional adcumulus growth of olivine crystals and generation of in situ crystallised poikilitic plagioclase with minor clinopyroxene. Filter-pressing of the

residual melt out of the lower crystallisation zone was most likely a trigger for the upward flow of the porous melt. The onset of this stage is recorded in the occurrence of plagiodunite, whose composition displays much lower Ca/Al ratios as compared to the chilled picrodolerite. In addition, plagiodunite shows a subtle enrichment in Sr and Eu (Fig. 12), which is expected for heterogeneous systems slightly enriched in cumulus plagioclase. This is an important argument for the cotectic nature of poikilitic plagioclase crystallised in situ, with the residual melt leaving the zone of initial adcumulus growth.

The magma-staging behavior of the upper part of the chamber continued, as demonstrated by the presence of both dykes and sill-like bodies of gabbronorite above the roof of the YDM. Despite some localised upper reversal signatures (Latypov, 2015; see V in Fig. 5) in the uppermost part of the YDM, the absence of a widespread roof succession (similar to the Upper Marginal Series of the Skaergaard intrusion) may be considered as indirect evidence for the high efficiency of the magma flowing process. This is because under the force of the emplaced magma, horizons of roof rocks crystallised downward collapsed. This inference is supported by the occurrence of large blocks of host country rocks and recrystallised hornfels inside the gabbronorite (Ariskin et al., 2013b; Kislov, 1998).

6.4.3. The third stage

Due to continuing growth of the cumulate pile, the upper crystal accumulation front reached the highest levels of the magma chamber, while its lower part was essentially solidified. This part of the Dovyren history is most speculative and questionable. In fact, one can suggest accumulation of the residual melts percolated from below at the upper boundary of the compacting cumulate pile. Assuming coupled effects of crystal compaction and continuing in situ crystallisation, the mafic melt residue had a subcotectic temperature (1180 °C or slightly lower), consistent with olivine Fo84-85 and plagioclase (An83-86), as observed in troctolites (Fig. 9). This slightly evolved melt could mix with the flowing magma. One cannot exclude that texturally inhomogeneous Cpx-containing troctolite in the upper part of the troctolite zone could originate at an initial stage of such mixing. Additional argument for the continuing melt expulsion from the upper part of the magma chamber follows from geochemical features of the olivine gabbronorite, whereby some of these rocks are more depleted in incompatible elements than the plagiodunite near the base of the YDM (Fig. 12D).

6.4.4. The fourth stage

The fourth stage characterises concluding magma transport phenomena in a residual and smaller magma reservoir, still including both cumulate piles and relatively liquid sub-chamber. Due to the fact that the efficiency of magma flow decreased, the chamber finally closed. Continuing heat loss, both from below and above, induced fractionation within the crystal-depleted melt, with most evolved rocks crystallising near the roof of the chamber (Fig. 9). From the other side, upward percolation of the residual melts from crystallising adcumulates was continuing at the same time, thus favouring mixing of the primitive magma with upper fractionated products. It is interesting that in a gabbronorite approximately 100 m below the upper contact, we found two distinct clusters of olivine compositions ranging from Fo68 to Fo79 (see data for the sample 09DV503-7 in Appendix B). This supports the proposed magma mixing hypothesis, as such contrasting olivine compositions are non-typical for most Dovyren rocks.

6.5. The mantle source

There is still uncertainty with respect to the nature of a probable mantle source of the YDM parental magmas, which are geochemically similar to the low-Ti basalts of the Synnyr suite, as well as being extremely enriched in radiogenic Sr and depleted in ε_{Nd}. Amelin et al. (1996) proposed a model which explains such anomalous characteristics as a result of melting of a metasomatized mantle peridotite shortly after subduction of sediments derived from an ancient (~2.4–2.8 Gyr) upper continental crust into a depleted lherzolitic mantle. Ariskin et al. (2015a) considered a different model, which is based on reconstructing the time-dependent evolution of $\varepsilon_{Nd}(t)$ for the YDM rocks until the inverse ε_{Nd}-trend (consistent with Sm/Nd ≅ 0.221 in a mantle protolith) intersects that of primitive mantle evolution with the initial mantle ratio of Sm/Nd = 0.350 (Kostitsyn, 2004). This reconstruction suggests that the anomalous mantle protolith formed at the Meso-Neoarchean boundary at ~2.8 Gyr, remained isolated from magmatic events for ~2 Gyr, and then reactivated at 728 Ma.

Geochemical similarities between the YDM rocks and those of granulites and granitoids from the southern margin of the Siberian craton suggest that the anomalous mantle could have formed within a subduction zone that existed at ~2.8 Gyr along the margin of the craton (Ariskin et al., 2015a). In alternative, the crust-like Sm/Nd ≅ 0.221 ratio in the proposed mantle protolith may argue for contamination by a primitive mantle (komatiite-like?) magma of even more ancient crustal materials. This is consistent with the slightly shifted oxygen isotope composition of olivine from the YDM ($\delta^{18}O = 5.8 \pm 0.1‰$; Fomin et al., 2013).

7. Conclusions

(1) The Yoko-Dovyren layered massif, associated mafic-ultramafic sills, and gabbronoritic dykes represent the intrusive constituent of the Upper Riphean Synnyr-Dovyren volcano-plutonic complex. Comparison of complete cross-sections of the thickest part of the largest intrusive body with those from this NE and SW terminations of the magmatic body reveal key differences in the lateral YDM architecture. The marginal domains are largely dominated by melanotroctolite to troctolite with relatively thin zones of plagiodunite, whereas the core mainly comprises a thick dunite zone. These differences, highlighted with petrochemical reconstructions, mineral chemistry, and COMAGMAT-5 calculations, indicate that the temperatures of the emplacing olivine-laden parental magmas in the central and peripheral parts of the intrusion ranged across 100 °C, approximately from 1290 °C (~11 wt% MgO, olivine Fo88) to 1190 °C (~8 wt% MgO, olivine Fo86).

(2) Based on the present thermodynamic modelling, the high-MgO magma in the centre was S-undersaturated, whereas its derivatives became S-saturated at the temperature of 1240 °C or below. This is consistent with geological observations that most sulphide-rich Cu-Ni ores were discovered in the sills and apophyses of plagioperidotite underneath the YDM, as well as at the periphery of the intrusion, where ultramafic rocks crystallised from a relatively evolved olivine gabbronorite magma.

(3) Because of the S-undersaturated character of the 'Fo88-magma', post-cumulus sulphide immiscibility could occur in crystallising primitive cumulates. As a result, a Ni-rich immiscible sulphide liquid is assumed to have originated directly in the cumulate pile, followed by its downwards migration to form a poorly-mineralised plagiodunite horizon. In the troctolite and gabbroic parts of the Dovyren chamber, sulphide immiscibility could occur at lower temperatures (probably around 1200 °C), generating Cu-rich sulphides, which gave rise to the sulphide-poor PGE-rich troctolite and PGE-rich anorthosite.

(4) The C-shaped distribution of TiO_2, K_2O, P_2O_5, and incompatible trace elements along cross-sections of the YDM reflects the depleted geochemistry of most Dovyren rocks compared to relatively thin contact zones, as well as associated ultramafic sills and gabbronorite dykes. Accounting for a marked misbalance between estimates of the average weighted compositions of the intrusion and proxies of the parental magmas, these data suggest that roughly 50–70% of complementary basaltic melts had to be expelled from the YDM during its consolidation.

(5) Two possible scenarios for the evolution of an open magmatic system are considered. One hypothesis takes into account that the formation of a thick sequence of Ol-rich cumulate pile should be accompanied by compaction and crystallisation, giving rise to upward migration and infiltration of the intercumulus melts. The second hypothesis suggests that the Dovyren chamber is a magma-staging system, through which large amounts of olivine gabbronorite magmas have passed, leaving behind a complementary melt-depleted succession of dunite, troctolite, and gabbroic cumulates. Here we propose a hybrid mechanism whereby these processes proceeded simultaneously. Our current model suggests that only minor fractionation of the Dovyren parental magmas occurred at the early to middle stages of solidification. However, one cannot exclude the possibility that at a final stage of evolution the magma chamber became closed, thus favouring in situ magma fractionation within the upper portion of the residual heterogeneous reservoir. This is consistent with the most evolved mineral compositions observed in olivine-free gabbronorite and quartz-pigeonite gabbro from the uppermost YDM.

(6) Reconstructions of the time-dependent evolution of $\varepsilon_{Nd}(t)$ for the YDM rocks suggest for the Dovyren magmas an anomalous mantle protolith formed at the Meso-Neoarchean boundary at ~2.8 Gyr. It remained isolated from magmatic events for ~2 Gyr, and then reactivated at 728 Ma.

Supplementary data to this article can be found online at https://doi.org/10.1016/j.lithos.2018.01.001.

Acknowledgements

We gratefully acknowledge thoughtful reviews by Steve Barnes, Rais Latypov and two anonymous reviewers, as well as constructive comments from the editor Andrew Kerr. We acknowledge support from AngloAmerican, BHP Billiton, Votorantim Metais, and the Australian Research Council through funding to CODES (University of Tasmania, Hobart, Australia) at the initial stage of this research (AMIRA project P962, 2007–2010); support from the Russian Science Foundation (RSF, grant No. 16-17-10129, 2016–2018); and support from the University of Tasmania through Visiting Scholarships to AAA in 2011 and 2014. MLF acknowledges support from the Australian Research Council through the Future Fellowship Scheme (FT110100241) and Foundation Project 2a of the Centre of Excellence for Core to Crust Fluid Systems. We thank Roland Maas (School of Earth Sciences, the University of Melbourne), Sebastian Meffre, Sarah Gilbert, and Paul Olin (University of Tasmania) for assistance with analytical work. Kirill Bychkov, Ian Woolword, Ludmila Zhitova, Dima Kamenetsky, Alexey Lygin, Jonas Mota e Silva, and Dmitry Orsoev assisted during fieldwork at the YDM in 2007. We also thank Evgeny Koptev-Dvornikov (Moscow State University, Russia) for his help with description of thin-sections, Masha Anosova and Kostya Ryazantsev (Vernadsky Institute, Moscow) for their assistance with sample preparation, and Kirill Bychkov for his work on the COMAGMAT-5 model. The authors would like to particularly acknowledge the contributions of late Dr. Eduard Konnikov who worked on this project in 2007–2011. We thank Candace S. O'Connor for careful editing of the submitted manuscript. This is contribution 1045 from the ARC Centre of Excellence for Core to Crust Fluid Systems (http://www.ccfs.mq.edu.au).

References

Amelin, Yu.V., Neymark, L.A., Ritsk, E.Yu., Nemchin, A.A., 1996. Enriched Nd–Sr–Pb isotopic signatures in the Dovyren layered intrusion (Eastern Siberia, Russia): evidence for source contamination by ancient upper-crust material. Chem. Geol. 129, 39–69.

Ariskin, A.A., Konnikov, E.G., Kislov, E.V., 2003. Modeling of the equilibrium crystallisation of ultramafic rocks with application to the problems of formation of phase layering in the Dovyren pluton, Northern Baikal region, Russia. Geochem. Int. 41, 107–129.

Ariskin, A.A., Konnikov, E.G., Danyushevsky, L.V., Kislov, E.V., Nikolaev, G.S., Orsoev, D.A., Barmina, G.S., Bychkov, K.A., 2009. The Dovyren Intrusive Complex: problems of petrology and Ni sulfide mineralization. Geochem. Int. 47, 425–453.

Ariskin, A.A., Danyushevsky, L.V., Bychkov, K.A., McNeill, A.W., Barmina, G.S., Nikolaev, G.S., 2013a. Modeling solubility of Fe-Ni sulfides in basaltic magmas: the effect of Ni in the melt. Econ. Geol. 108, 1983–2003.

Ariskin, A.A., Kostitsyn, Yu.A., Konnikov, E.G., Danyushevsky, L.V., Meffre, S., Nikolaev, G.S., McNeill, A., Kislov, E.V., Orsoev, D.A., 2013b. Geochronology of the Dovyren Intrusive Complex, Northwestern Baikal area, Russia, in the Neoproterozoic. Geochem. Int. 51, 859–875.

Ariskin, A.A., Danyushevsky, L.V., Konnikov, E.G., Maas, R., Kostitsyn, Yu.A., McNeill, A., Meffre, S., Nikolaev, G.S., Kislov, E.V., 2015a. The Dovyren Intrusive Complex (Northern Baikal region, Russia): isotope-geochemical markers of contamination of parental magmas and extreme enrichment of the source. Russ. Geol. Geophys. 56, 411–434.

Ariskin, A.A., Nikolaev, G.S., Danyushevsky, L.V., Kislov, E.V., Malyshev, A., Barmina, G.S., 2015b. New type of low-sulfide PGE mineralization in primitive troctolites from the Yoko-Dovyren layered massif. Proceedings of XII All-Russian Petrographic Conference vol. 1, pp. 289–291 (Petrozavodsk, Karelia, (in Russian)).

Ariskin, A.A., Danyushevsky, L.V., Kislov, E.V., Nikolaev, G.S., Fiorentini, M., Gilbert, S., Goemann, K., Malyshev, A., 2016. Cu-Ni-PGE fertility of the Yoko-Dovyren layered massif (Northern Transbaikalia, Russia): thermodynamic modeling of sulfide compositions in low mineralized dunites based on quantitative sulfide mineralogy. Mineral. Deposita 51, 993–1011.

Balykin, P.A., Polyakov, G.V., Bognibov, V.I., Petrova, T.E., 1986. Proterozoic Ultrabasic-basic Rock Associations of the Baikal–Stanovoi Area. Nauka, Novosibirsk (in Russian).

Barnes, S.J., Mungall, J.E., LeVaillant, M., Godel, B., Lesher, C.M., Holwell, D., Lightfoot, P.C., Krivolutskaya, N., Wei, B., 2017. Sulfide-silicate textures in magmatic Ni-Cu-PGE sulfide ore deposits: disseminated and net-textured ores. Am. Mineral. 102, 473–506.

Bolikhovskaya, S.V., Yaroshevskii, A.A., Koptev-Dvornikov, E.V., 2007. Simulation of the Geochemical Structure of the Ioko-Dovyren Layered Intrusion. 45. Northwestern Baikal Area Geochemistry International, pp. 519–537.

Denisova, M.V., 1961. Copper-nickel sulfide mineralization in a mafic-ultramafic massif of the Baikal Folded area. Proceedings on Geology and Mineralogy of Ore Deposits of USSR (New Series 60). VSEGEI, Leningrad, pp. 37–46 (in Russian).

Distler, V.V., Stepin, A.G., 1993. Low-sulfide PGE-bearing unit of the Yoko–Dovyren layered ultrabasic-basic intrusion (Northern Baikal region). Dokl. Akad. Nauk 328, 498–501.

Efimov, A.A., Potapova, T.A., 2003. Geochemistry of strontium in layered intrusions: a petrogenetic aspect (the example of the Ioko-Dovyren and some other complexes). Geochem. Int. 41, 753–769.

Ernst, R.E., Bleeker, W., 2010. Large igneous provinces (LIPs), giant dyke swarms, and mantle plumes: significance for breakup events within Canada and adjacent regions from 2.5 Ga to present. Can. J. Earth Sci. 47, 695–739.

Ernst, R.E., Hamilton, M.A., Söderlund, U., Hanes, J.A., Gladkochub, D.P., Okrugin, A.V., Kolotilina, T., Mekhonoshin, A.S., Bleeker, W., LeCheminant, A.N., Buchan, K.L., Chamberlain, K.R., Didenko, A.N., 2016. Long-lived connection between southern Siberia and northern Laurentia in the Proterozoic. Nat. Geosci. 9:464–469. https://doi.org/10.1038/NGEO2700.

Fomin, I.S., Nikolaev, G.S., Ariskin, A.A., 2013. Estimates of redox conditions and temperatures of closure of the olivine-spinel system in cumulate rocks of the Ioko-Dovyren layered intrusion. Proceedings of 12th SGA Biennial Meeting "Mineral deposit research for a high-tech world". vol. 3, pp. 982–984 12–15th August 2013, Uppsala, Sweden.

Grudinin, M.I., 1963. Geology and petrology of the Dovyren gabbro-peridotite massif, Northern Baikal area. Geology and Geophysics 4, 78–91 (in Russian).

Grudinin, M.I., 1965. Petrography of the Nyurundukan and Dovyren gabbro-peridotite massifs, Northern Baikal area. In: Afanasiev, G.D., Belov, I.V. (Eds.), Petrography of Eastern Siberia. vol. 3. Nauka, Moscow, pp. 5–112 (in Russian).

Gurulev, S.A., 1965. Geology and Genesis of the Yoko-Dovyren Gabbro-peridotite Massif. Nauka, Moscow (in Russian).

Gurulev, S.A., 1983. Genesis of Layered Mafic Intrusions. Nauka, Moscow (in Russian).

Heaman, L.M., LeCheminant, A.N., Rainbird, R.H., 1992. Nature and timing of Franklin igneous event, Canada: implications for a Late Proterozoic mantle plume and the break-up of Laurentia. Earth Planet. Sci. Lett. 109, 117–131.

Jowitt, S.M., Ernst, R.E., 2013. Geochemical assessment of the metallogenic potential of Proterozoic LIPs of Canada. Lithos 174, 291–307.

Kislov, E.V., 1998. The Yoko-Dovyren Layered Massif. BNTsRAN, Ulan-Ude (in Russian).

Kislov, E.V., 2010. The nickel reserve of Russia: the Northern Baikal nickel-fertile province. Globus (Geology and Business) 13, 30–37 (in Russian).

Kislov, E.V., Konnikov, E.G., Orsoev, D.A., Pushkarev, E.V., Voronina, L.K., 1995. Constraints on the genesis of low-sulphide PGE mineralization at the Ioko-Dovyren layered massif, Northern Transbaikalia, Russia. In: Pasava, J., Kribek, B., Zak, K. (Eds.), Mineral Deposits: From Their Origin to Their Environmental Impacts. AA Balkema, Rotterdam, pp. 121–124.

Konnikov, E.G., 1986. Differentiated Ultrabasic-basic Complexes in the Precambrian Rocks of Transbaikalia. Nauka, Novosibirsk (in Russian).

Konnikov, E.G., Kislov, E.V., Orsoev, D.A., 1994. Yoko-Dovyren layered pluton and related mineralization, Northern Transbaikalia (in Russian). Geol. Ore Deposits 36, 545–553.

Konnikov, E.G., Tsygankov, A.A., Vrublevskaya, T.T., 1999. The Baikal–Muya Volcanic-Plutonic Belt: Lithotectonic Complexes and Geodynamics. GEOS, Moscow (in Russian).

Konnikov, E.G., Meurer, W.P., Neruchev, S.S., Prasolov, E.M., Kislov, E.V., Orsoev, D.A., 2000. Fluid regime of platinum group elements (PGE) and gold-bearing reef formation in the Dovyren mafic–ultramafic layered complex, Eastern Siberia, Russia. Mineral. Deposita 35, 526–532.

Kostitsyn, Yu.A., 2004. Terrestrial and chondritic Sm–Nd and Lu–Hf isotopic systems: are they identical? Petrology 12, 397–411.

Kostitsyn, Yu.A., 2007. Relationships between the chemical and isotopic (Sr,Nd, Hf, and Pb) heterogeneity of the mantle. Geochem. Int. 45, 1173–1196.

Latypov, R.M., 2015. Basal reversals in mafic sills and layered intrusions. In: Charlier, B., Namur, O., Latypov, R., Tegner, C. (Eds.), Layered Intrusions, 1st ed. Springer International Publishing, Weteringschans, pp. 259–293 Springer. (New York City: Springer. 9401796521, 9789401796521).

Li, Z.X., Bogdanova, S.V., Collins, A.S., Davidson, A., Waele, B.De., Ernst, R.E., Fitzsimons, I.C.W., Fuck, R.A., Gladkochub, D.P., Jacobs, J., Karlstrom, K.E., Lu, S., Natapov, L.M., Pease, V., Pisarevsky, S.A., Thrane, K., Vernikovsky, V., 2008. Assembly, configuration, and break-up history of Rodinia: a synthesis. Precambrian Res. 160, 179–210.

Manuilova, M.M., Zarubin, V.V., 1981. Precambrian Volcanogenic Rocks of the Northern Baikal Region. Nauka, Leningrad (in Russian).

Metelkin, D.V., Kazansky, A.Yu., Vernikovsky, V.A., 2009. Paleomagnetic Evidence for Siberian Plate Tectonics from Rodinia through Pangaea to Eurasia. In: Ferrari, D.M., Guiseppi, A.R. (Eds.), Geomorphology and Plate Tectonics. Nova Science Publishers, NY, pp. 159–236.

Mungall, J.E., Brenan, J.M., 2014. Partitioning of platinum-group elements and Au between sulfide liquid and basalt and the origins of mantle-crust fractionation of the chalcophile elements. Geochim. Cosmochim. Acta 125, 265–289.

Neimark, L.A., Rytsk, E.Yu., Levchenkov, O.A., Komarov, A.N., Yakovleva, S.Z., Nemchin, A.A., Shuleshko, I.K., Korikovskii, S.P., 1990. Paleoproterozoic-Early Riphean rocks in the Olokit Complex: U-Pb zircon dates. In: Shemyakin, V.M. (Ed.), Precambrian Geology and Geochronology of the Siberian Platform and its Surroundings. Nauka, Leningrad, pp. 206–222 (in Russian).

Orsoev, D.A., Kislov, E.V., Konnikov, E.G., Kanakin, S.V., Kulikova, A.B., 1995. Localization appropriateness and composition specific features of platinum-bearing horizons of the Ioko-Dovyren layered massif (Northern Transbaikalia). Dokl. Akad. Nauk 340, 225–228.

Orsoev, D.A., Rudashevskii, N.S., Kretser, Yu.L., Konnikov, E.G., 2003. Precious metal mineralization in low-fulfide ores of the Ioko–Dovyren layered massif, Northern Baikal region. Transactions (Doklady) of the Russian Academy of Sciences/Earth Science Section 390, 545–549.

Parfenov, L.M., Badarch, G., Berzin, N.A., et al., 2010. Chapter 1 (Introduction). In: Nokleberg, W.J. (Ed.), Metallogenesis and tectonics of northeast Asia: U.S. Geological Survey Professional Paper 1765, pp. 1–36.

Pertsev, N.N., Shabynin, L.I., 1979. Skarn, carbonate,and brucite xenoliths of the Yoko–Dovyren massif. In: Korzhinskiy, D.S., Gurulev, S.A., Zotov, I.A. (Eds.), Contact Processes and Mineralization in the Gabbro-peridotite Intrusions. Nauka, Moscow, pp. 85–96 (in Russian).

Pisarevsky, S.A., Natapov, L.M., Donskaya, T.V., Gladkochub, D.P., Vernikovsky, V.A., 2008. Proterozoic Siberia: a promontory of Rodinia. Precambrian Res. 160, 66–76.

Plechov, P.Y., Shishkina, T.A., Ermakov, V.A., Portnyagin, M.V., 2008. Formation conditions of allivalites, olivine-anorthite crystal enclaves, in the volcanics of the Kuril-Kamchatka arc. Petrology 16, 232–260.

Polyakov, G.V., Tolstykh, N.D., Mekhonoshin, A.S., Izokh, A.E., Podlipskii, M.Yu., Orsoev, D.A., Kolotilina, T.B., 2013. Ultramafic–mafic igneous complexes of the Precambrian East Siberian metallogenic province (southern framing of the Siberian craton): age, composition, origin, and ore potential. Russ. Geol. Geophys. 54, 1319–1331.

Pushkarev, E.V., Votyakov, S.L., Chashchukhin, I.S., Kislov, E.V., 2004. Olivine–chromspinel oxythermobarometry of ultramafic rocks of the Ioko–Dovyren layered massif. Transactions (Doklady) of the Russian Academy of Sciences/Earth Science Section 395, 266–270.

Ripley, E.M., Li, C., 2013. Sulfide saturation in mafic magmas: is external sulfur required for magmatic Ni-Cu-(PGE) ore genesis? Econ. Geol. 108, 45–58.

Rudashevsky, N.S., Kretser, Yu.L., Orsoev, D.A., Kislov, E.V., 2003. Palladium-platinum mineralization in copper-nickel vein ores in the Ioko-Dovyren layered massif. Dokl. Earth Sci. 391A, 858–861.

Rytsk, E.Yu., Shalaev, V.S., Rizvanova, N.G., Krymskii, R.Sh., Makeev, A.F., Rile, G.V., 2002. The Olokit Zone of the Baikal Fold Region: new isotopic geochronological and geochemical data. Geotectonics 36, 24–35.

Rytsk, E.Yu., Kovach, V.P., Kovalenko, V.I., Yarmolyuk, V.V., 2007. Structure and evolution of the continental crust in the Baikal Fold region. Geotectonics 41, 440–464.

Sun, S.-S., McDonough, W.F., 1989. Chemical and isotopic systematics of oceanic basalts: implications for mantle composition and processes. In: Saunders, A.D., Norry, M.J. (Eds.), Magmatism in the Ocean Basins. vol. 42. Geological Society London Special Publications, London, pp. 313–345.

Tolstykh, N.D., Orsoev, D.A., Krivenko, A.P., Izokh, A.E., 2008. Noble-metal Mineralization in Layered Ultrabasic-basic Massifs of the Southern Siberian Platform. Parallel, Novosibirsk (in Russian).

Wenzel, T., Baumgartner, L.P., Brugmann, G.E., Konnikov, E.G., Kislov, E.V., 2002. Partial melting and assimilation of dolomitic xenoliths by mafic magma: the Ioko-Dovyren Intrusion (North Baikal region, Russia). J. Petrol. 43, 2049–2074.

Yaroshevskii, A.A., Ionov, D.A., Mironov, Yu.V., Koptev-Dvornikov, E.V., Abramov, A.V., Krivoplyasov, G.S., 1982. Petrography and geochemistry of the Yoko-Dovyren dunite–troctolite–gabbro–norite layered massif, Northern Baikal area. In: Bogatikov, O.A. (Ed.), Petrology and Ore Potential of Natural Rock Associations. Nauka, Moscow, pp. 86–117 (in Russian).

Yaroshevskii, A.A., Bolikhovskaya, S.V., Koptev-Dvornikov, E.V., 2006. Geochemical structure of the Yoko–Dovyren layered dunite-troctolite-gabbro-norite massif, Northern Baikal area. Geochem. Int. 44, 953–964.